JPL PUBLICATION 77-62, VOLUME I

Viking Lander Camera Radiometry Calibration Report

National Aeronautics and
Space Administration

Jet Propulsion Laboratory
California Institute of Technology
Pasadena, California 91103

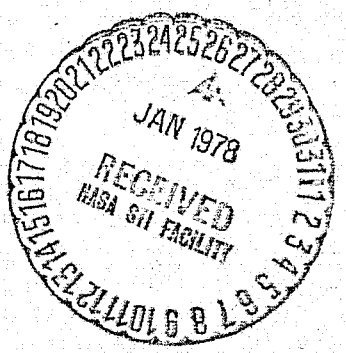

TECHNICAL REPORT STANDARD TITLE PAGE

1. Report No. JPL Pub. 77-62	2. Government Accession No.	3. Recipient's Catalog No.
4. Title and Subtitle Viking Lander Camera Radiometry Calibration Report (Volume I)		5. Report Date November 1, 1977 6. Performing Organization Code
7. Author(s) M. R. Wolf/ D. L. Atwood/M. E. Morrill		8. Performing Organization Report No.
9. Performing Organization Name and Address JET PROPULSION LABORATORY California Institute of Technology 4800 Oak Grove Drive Pasadena, California 91103		10. Work Unit No. 11. Contract or Grant No. NAS 7-100 13. Type of Report and Period Covered JPL Publication
12. Sponsoring Agency Name and Address NATIONAL AERONAUTICS AND SPACE ADMINISTRATION Washington, D.C. 20546		14. Sponsoring Agency Code

15. Supplementary Notes

16. Abstract

This report describes the test methods and data reduction techniques used to determine and remove instrumental signatures from Viking Lander Camera Radiometry Data. Included are detailed descriptions of all tests and reduced data. Tables of gain, offset, and calibration constants included in the figures allow the reader to remove the instrumental signature from Viking Lander Flight Radiometry Data.

17. Key Words (Selected by Author(s))	18. Distribution Statement
Viking Mars 1975 Project Spacecraft Design, Testing and Performance Spacecraft Instrumentation Optics Lunar and Planetary Exploration (Advanced)	Unclassified - Unlimited

19. Security Classif. (of this report)	20. Security Classif. (of this page)	21. No. of Pages	22. Price
Unclassified	Unclassified	90	

HOW TO FILL OUT THE TECHNICAL REPORT STANDARD TITLE PAGE

Make items 1, 4, 5, 9, 12, and 13 agree with the corresponding information on the report cover. Use all capital letters for title (item 4). Leave items 2, 6, and 14 blank. Complete the remaining items as follows:

3. Recipient's Catalog No. Reserved for use by report recipients.

7. Author(s). Include corresponding information from the report cover. In addition, list the affiliation of an author if it differs from that of the performing organization.

8. Performing Organization Report No. Insert if performing organization wishes to assign this number.

10. Work Unit No. Use the agency-wide code (for example, 923-50-10-06-72), which uniquely identifies the work unit under which the work was authorized. Non-NASA performing organizations will leave this blank.

11. Insert the number of the contract or grant under which the report was prepared.

15. Supplementary Notes. Enter information not included elsewhere but useful, such as: Prepared in cooperation with... Translation of (or by)... Presented at conference of... To be published in...

16. Abstract. Include a brief (not to exceed 200 words) factual summary of the most significant information contained in the report. If possible, the abstract of a classified report should be unclassified. If the report contains a significant bibliography or literature survey, mention it here.

17. Key Words. Insert terms or short phrases selected by the author that identify the principal subjects covered in the report, and that are sufficiently specific and precise to be used for cataloging.

18. Distribution Statement. Enter one of the authorized statements used to denote releasability to the public or a limitation on dissemination for reasons other than security of defense information. Authorized statements are "Unclassified—Unlimited," "U.S. Government and Contractors only," "U.S. Government Agencies only," and "NASA and NASA Contractors only."

19. Security Classification (of report). NOTE: Reports carrying a security classification will require additional markings giving security and downgrading information as specified by the Security Requirements Checklist and the DoD Industrial Security Manual (DoD 5220.22-M).

20. Security Classification (of this page). NOTE: Because this page may be used in preparing announcements, bibliographies, and data banks, it should be unclassified if possible. If a classification is required, indicate separately the classification of the title and the abstract by following these items with either "(U)" for unclassified, or "(C)" or "(S)" as applicable for classified items.

21. No. of Pages. Insert the number of pages.

22. Price. Insert the price set by the Clearinghouse for Federal Scientific and Technical Information or the Government Printing Office, if known.

JPL PUBLICATION 77-62, VOLUME I

Viking Lander Camera Radiometry Calibration Report

Michael R. Wolf
David L. Atwood
Michael E. Morrill

November 1, 1977

National Aeronautics and
Space Administration

Jet Propulsion Laboratory
California Institute of Technology
Pasadena, California 91103

PREFACE

The work described in this two-volume report was conducted in the Image Processing Laboratory by the Earth and Space Sciences Division of the Jet Propulsion Laboratory.

Volume I describes the test methods and data reduction techniques used to determine and remove instrumental signatures from Viking Lander Camera Radiometry Data.

Volume II contains voluminous plots and tables of responsivity for diodes of all cameras and is published separately as a microfiche package. When processed, copies of the microfiche package may be obtained from the Technical Information and Documentation Division, Jet Propulsion Laboratory, 4800 Oak Grove Drive, Pasadena, California 91103.

ACKNOWLEDGMENTS

The efforts of many people were directed toward making this test program meaningful and complete to the last detail. Among those who contributed to the success of the tests were: Ed Green, Jack Donahue, and Cliff Maxwell of ITEK, Phil Avrin of Martin Marietta Aerospace (MMA), and Steve Wall of Langley Research Center (LRC).

ABSTRACT

This report describes the test methods and data reduction techniques used to determine and remove instrumental signatures from Viking Lander Camera Radiometry Data. Included are detailed descriptions of all tests and reduced data. Tables of gain, offset, and calibration constants included in the figures allow the reader to remove the instrumental signature from Viking Lander Flight Radiometry Data.

CONTENTS

CONTENTS (Continued)

CONTENTS (Continued)

Figures

CONTENTS (Continued)

Figures

1. HISTORICAL REVIEW

The Image Processing Laboratory (IPL) was not originally involved in the planning which led to the development of project schedules for design, construction and testing of the Viking Lander camera. In early 1973 IPL was given the task of second order processing support for the Viking Lander mission, which would include software to determine absolute radiometric and geometric information for Viking Lander images (so-called 'decalibration' software). This meant that the cameras would have to undergo much more extensive tests than those already planned which would 'calibrate' their radiometric and geometric characteristics. The amount of operating time on each camera which was required to provide IPL the necessary data to write the appropriate software was several times the amount already budgeted (both in time and money). In a Lander Imaging Team meeting in August, 1973, Bill Green, Andy Young and Mike Wolf presented the IPL proposal for calibration testing. At first rejected by project management as too consuming of vital camera scan 'life cycles', a reduced series

of tests was approved and checked out on the 'QUAL' camera, a non-flight unit, in the 'Pathfinder' series of tests in December, 1973. Much was learned from this series of tests and the final test configuration was firmed up. The flight cameras began IPL 'calibration tests' in January, 1974, and continued through the middle of that year. In all, five flight cameras completed the complete sequence of IPL tests: FC-1B, FC-2B, FC-2A, FC-3A and SPARE.

2. SCOPE OF REPORT

Although the flight cameras underwent some testing for radiometric response at MMA and KSC, IPL did not reduce most of this data. Instead, all calibration files were constructed using data from the ITEK component level testing. There were two reasons for this. First, the test environment at ITEK allowed a more iterative or "Let's try it and change it if it doesn't work" operational environment, due mainly to the simpler equipment required to operate the camera when it is not an integral part of the spacecraft. This environment was more conducive to the acquiring of good (e.g., unsaturated) test data. Also, the push was on to develop our camera model and get the cameras characterized at the earliest opportunity, and the ITEK data was our first opportunity. For

these reasons, the IPL radiometric calibration effort and this report, will consider only those tests taken at ITEK.

Included in Volume I of this report is a discussion of the radiometric model and the method for calculating calibration constants. All the tests are described and sample calculations outline data reduction methods. Results for each test are presented.

Included in Volume II are absolute responsivity curves and tables of the responsivity for all diodes, all flight cameras; all the 'IPL calibration data transmittal reports'; spectral irradiance tables for both standard lamps used during calibration; the solar spectrum irradiance function; spectrophotometer curves for a representative internal calibration lamp, the complete calibration files for all cameras; and the calibration results for the ITEK radiometric sources.

3. THE CAMERA

For the purposes of radiometric calibration, the Viking Lander camera will be assumed to be perfectly modeled by the 'black box' diagram shown in Figure 1.

The first 'black box' is the photo diode/load resistor combination whose response to the incident light is S volts and whose 'dark current' (converted to a voltage by the load resistor) is

d volts. The total output is then S+d. The next 'black box' is the dark current subtractor. The output from this box is S volts. After this, the signal passes through the offset adder, whose output is then (S+f) volts. The final black box is the amplifier, of gain G in units of DN/volt. The final output is then G(S+f). If this value is truncated to an integer, we have the digital data number output from the camera, or:

$$DN = G(S+f) \tag{1}$$

The signal voltage S can be represented as:

$$S = \int_0^\infty R_\lambda S_\lambda \, d\lambda \tag{2}$$

where

S is the signal voltage developed across the load resistor in volts;

R_λ is the responsivity of the total camera system expressed in VOLT-CM^2-SR-MICROWATT^{-1}

S_λ is the spectral radiance of the source being imaged by the camera, in MICROWATT-CM^{-2}-SR^{-1}-NM^{-1}

The offset adder can add any of 32 discrete voltage levels to its input. These levels are numbered 0 through 31. The values range from approximately +0.2 volts to -4.3 volts, in equal steps of approximately 0.14 volts. Figure 2 is the table of actual values of all 32 steps for camera 1, Lander 1 (FC-1B).

The amplifier has six discrete gain settings numbered 0, 1, 2, 3, 4, 5 (gain 0 is the highest or most strongly amplifying gain and gain 5 is the lowest). Figure 3 is a table of the room temperature gain values for camera 1, Lander 1 (FC-1B), in units of DN/volt.

The problem of completely modeling the camera, then, is reduced to determining all the parameters of the model, i.e., we must determine R at all wavelengths for all diodes, f for all 32 offset steps, and G for all six gain steps. Since R, f, and G may be functions of temperature, we should do this for several temperatures which bracket those expected on Mars.

The problem of determining R_λ for each channel has been made considerably easier for us as the relative responsivity of each diode as a component was measured by a scanning monochrometer at MMA. The overall camera relative responsivity for a given channel is just:

$$R_\lambda^R = T_\lambda^{CC}\, T_\lambda^W\, R_\lambda^M\, T_\lambda^L\, T_\lambda^C\, R_\lambda^D \qquad (3)$$

where

R_λ^R is the overall <u>relative</u> camera responsivity for a given channel (as distinct from R_λ which is the <u>absolute</u> responsivity. Obviously, $R_\lambda = R_o \cdot R_\lambda^R$ where R_o is a constant to make the units come out right.); T_λ^{CC}, T_λ^W, T_λ^L, T_λ^C are the

transmissions of the contamination cover, window, lens and PSA cover glasses respectively; R_λ^M is the reflectance of the mirror; and R_λ^D is the diode component-level relative responsivity determined by MMA.

Let's take this relative responsivity R_λ^R and normalize it to 1.0 at its highest value and call it R_λ^*. Now we can write:

$$R_\lambda = R_o \cdot R_\lambda^* \tag{4}$$

where R_λ is the absolute channel responsivity, R_λ^* is the peak-normalized channel responsivity, and R_o is the peak (maximum) value of R_λ. We know R_λ^* so we must only determine the constant R_o to completely determine R_λ.

Assume we are imaging a standard diffuse source, whose spectral radiance, S_λ, is known at all wavelengths. The camera response, S, is just:

$$S = R_o \int_o^\infty R_\lambda^* S_\lambda d\lambda \equiv R_o L \tag{5}$$

where

$$L \equiv \int_o^\infty R_\lambda S_\lambda d\lambda \tag{6}$$

Equation (6) is the definition of 'diode lumens' in analogy with the definition of the photometric quantity the 'lumen' which relates to the response of the human eye to a light source. In the case of 'diode lumens' the responsivity curve used is just the

normalized responsivity of the channel in question instead of the responsivity curve of the human eye. A photometer expresses its results in quantities related to the human eye response (lumens, footlamberts, etc.). To accomplish this, a photometer has a filter stack which has been carefully 'trimmed' to closely approximate the international 'photoptic curve' or human eye responsivity curve (see Allen, Astrophysical Quantities, p. 105). The calibration process described below will allow us to use a generalized version of the 'lumen' which I call 'diode lumens', to express our results. It is the only meaningful way to express the response of a radiometer to a light source whose spectral radiance function, S_λ, is completely unknown.

It is clear that if we image a source of known spectral distribution, i.e., S_λ is known, then the integral in Equation (6) is calculable. From Equation (1) we can solve for S:

$$S = \frac{DN}{G} - f \tag{7}$$

where DN is the digital data number of the image of the source, G is the gain in DN/volt, and f is the offset voltage used.

Combining Equations (5), (6), and (7), we get:

$$R_o = \left(\frac{DN}{G} - f\right) \cdot \frac{1}{L} \tag{8}$$

since DN, G, and f are all known and we can calculate L (since we know S_λ), then we can calculate R_o.

Now that we have determined R_o, let's imagine that we are imaging an unknown scene (i.e., S_λ is not known). Equation (8) can be re-arranged thusly:

$$L = \left(\frac{DN}{G} - f\right) \cdot \frac{1}{R_o} \tag{9}$$

The value of R_o that we have determined for a particular scene (e.g., standard lamp) is valid for any scene, and in fact will allow us to calculate the 'diode lumens' for an unknown scene spectral distribution, providing we know the parameters DN, G, and f. We may rewrite Equation (9) thusly:

$$L = \left(\frac{DN}{G} - f\right) \cdot C_I^K \tag{10}$$

where

$$C_I^K \equiv 1/R_o \tag{11}$$

The superscript K denotes which channel (K runs from 1 to 12) and the subscript I denotes contamination cover open or closed (I takes on only two values: 1 or 2).

The determination of C_I^K values for five flight cameras, for all diodes, for three temperatures, along with the G and f values already described, completes the radiometric characterization of the cameras.

The subject of noise is treated in more detail in a later section (see 'The Tests in Outline', Coherent Noise Test), but the

noise generated by the dark current subtractor is properly discussed here in the camera section.

The dark current subtractor is designed to sample the dark current and integrate it to obtain a good average value during mirror retrace once every 64 scans. This constant value is then subtracted from the diode output for the next 64 scans, until a new sample is taken. The problem with this is that it is accomplished with a 'sample and hold' circuit whose 'hold' function is imperfect. The value out of the 'hold' circuit should remain constant, but in fact drifts slightly. This drift affects the image data because the value being subtracted is changing even if the light intensity in the scene may be constant. This causes a 'ramp' or 'sawtooth' function to appear in the image which is periodic every 64 camera scan lines. Even if we disable the dark current subtractor, the problem is still with us, because the disabling is accomplished by shorting the input to the sample circuit, not by disconnecting the hold-subtract circuit. Figures 4 and 5 show this effect for a survey diode at high and low data rate, respectively. The shading in the low data rate image is explained by the fact that at low data rate the dark current sample is taken every scan line instead of every 64 scan lines. Hence, the shading pattern repeats itself every scan line instead of every 64 scan lines (scan lines are horizontal in Figs. 4 and 5). Since the problem occurs before the amplifier, the effect on the image

is gain-dependent. For channels where signal-to-coherent-noise ratio is already high (e.g., SURVEY diode), at high gain settings, this dark current subtractor noise is the dominant noise source.

4. THE TESTS IN OUTLINE

In this section, all IPL-designed tests are briefly mentioned; those that survived 'Pathfinder' testing and were run on the flight landers are noted.

4.1 Gain Test

Figure 1 shows the block diagram camera model. Note the input line labeled 'test connector'. This test connector allowed us to enter a signal to the Video Processing Electronics (VPE) as though it had come from the PSA. In this way, the amplifiers' response to a series of different D.C. voltage levels could be monitored. Usually four or five steps were chosen that would not cause saturation yet would span the dynamic range of the particular gain setting chosen. These voltage levels are called the 'stimuli'. For each of these 'stimuli' the camera was commanded to take a picture, with a black cloth over the camera to prevent light from adding to the 'stimulus'. The 'response' to the 'stimulus' was chosen to be the mean of a 30x30 pixel area in the resulting image. This gives us the end-to-end response of the entire camera system (excluding PSA) from PSA output through and including the A/D converter. When 'stimulus' is plotted against 'response', a straight line results,

whose slope is the effective gain value for that gain step, in units of DN/volt.

This test survived to flight level testing.

4.2 Offset Test

This test is very similar to the gain test with the exception that the voltage input to the test connector was constant and the offset step was changed between images. The D.C. voltage was only changed every four or five images to prevent saturation as the offsets were increased. Thus, the 'stimulus' was the offset step values themselves. The 'response' was again, as in the gain test, the mean DN of a 30x30 pixel patch in the resulting images. When 'stimulus' is plotted against 'response', a straight line should result, whose slope is equal to the mean voltage increment between offset steps.

This test survived to flight testing.

4.3 'Chalk Block' Absolute Calibration Test

A magnesium carbonate block (magnesium carbonate is noted for its nearly lambertian photometric function) of 96.8% reflectance was illuminated at a 20° incidence angle (20° off normal incidence) at a distance of 50 cm.

For the calculation of the calibration constants, C_I^K, the $MgCO_3$ reflectance was taken to be 100%. Hence, all the C_I^K values

are calculated relative to $MgCO_3$. The lamp used was Eppley Standard Lamp S/N 1569. This lamp is traceable to NBS. Its spectral distribution is shown in Figure 6. Images of the illuminated chalk block were taken with all diodes, and a 30x30 pixel patch in the image was averaged to obtain the 'response'. The 'stimulus' is the radiance or brightness of the chalk block (which is just the irradiance divided by π). With a knowledge of the gain and offset values used to take a given image, the calibration constant, C_I^K, can be calculated from Equations (5), (6), (8) and (11).

This test was not run during the 'Pathfinder' series of tests, but rather was developed during flight testing as a slight modification to Test 4.6 below.

4.4 'RTC' Absolute Calibration Test

This test is identical to 4.3 except that the target was a Viking Lander Reference Test Chart instead of a magnesium carbonate block.

This test survived to flight testing, but IPL did not reduce the test data, as Test 4.3 provides identical data. Also, there was a serious question about the accuracy of the photometric function of the RTC at the time the test data had to be reduced. (See Wall et al., 1975.)

4.5 'Radiometric Source' Absolute Calibration Test

This test is identical to 4.3 or 4.4, except that the target was the 'ITEK Radiometric Source'.

This test did not survive to flight testing.

4.6 Relative Spectral Response Test

This test is identical to 4.3, except that a number of images of the carbonate block were taken through various interference filters, in an attempt to determine the relative spectral responsivity of the various diodes.

The filters actually used, though of high quality, did not have narrow enough bandpass to give useful data.

This test survived to flight testing, but for the reason given above, and for reasons of time, IPL did not reduce the data.

4.7 Internal Calibration Test

In this test the internal calibration mode was commanded, for both the medium and high intensity levels for the calibration lamp, for all diodes, for several temperatures. This data is used as a baseline to determine the changes in the cameras during flight.

4.8 Color Response as a Function of Elevation Angle Test

In this test, the camera imaged the ITEK Radiometric Source at a number of elevation angles, in an attempt to see if the

transmission of the optical system was a function of elevation. For one camera, the test was repeated with the contamination cover closed.

This test survived to flight testing.

4.9 Laser Test

The test was an attempt to spot-check the responsivity function of the diodes by using a highly monochromatic source, i.e., a 2 mw He-Ne laser. Unfortunately, due to troubles with the laser power meter, the results were unusable.

This test survived to flight testing, but IPL did not reduce the data.

4.10 Polarization Test

This test is identical to 4.6, but instead of using color filters, a polarizer was used. Only two images were taken: one with the transmission axis of the polarizer horizontal and one with it vertical. The data was only reduced for one camera. No polarization effect was seen.

This test survived to flight testing.

4.11 Coherent Noise Test

'Dark current' images were taken with all diodes, at several temperatures, with the dark current subtractor both on and off. A 'dark current' image is obtained by excluding all light to the

camera by covering it with a black cloth and turning out the room lights. The images thus obtained were processed by a one-dimensional Fourier transform program to determine the major coherent noise components in the camera system.

This test survived to flight camera testing.

4.12 Point Spread Function Test

In this test images were taken of an unresolved pin hole source at two different gain settings, with all diodes, to determine the point spread function.

This test survived to flight camera testing.

4.13 Sine and Square Wave Response

Sine and square wave targets of various frequencies were imaged by the BB1 diode at room temperature and again at -18^{o}C. The source which backlit the targets was not of uniform brightness, so a program which would correct for this effect was written. This program simply divided the backlit image of the sine or square wave transparency by the image of the backlighting source with the transparency removed. Figure 7 is the image of a square wave, before the 'flattening' program was applied, and Figure 8 shows the same image after correction for the non-uniform source. Figure 9 is the MTF function calculated from the image in Figure 8. Figure 7A is the image of a sine wave target. Note the moire

effect (or 'aliasing') which is due to the undersampling of the Viking Lander camera.

Due to the difficulty or impossibility of interpreting severely aliased data, this test did not survive to flight testing.

5. REDUCED FLIGHT CAMERA TESTS

5.1 Gain Test

The basic features of the gain test are outlined in Section 4.1 of this report. Basically, we put various D.C. levels into the amplifier input (output of the PSA) and commanded the camera to take a minimum size picture (2.5°). Data reduction consisted of computing the mean DN of a 30x30 pixel patch in the image, and plotting these mean values as a function of the input voltage. This was done for each of the six gain steps, for each camera, at each of three temperatures. The slopes of these linear plots of mean DN vs. voltage are numerically equal to the amplifier gains. These slopes were obtained by the method of least squares. Figure 10 shows a typical plot for gain step #3, Camera FC-1B (Lander 1, Camera 1). Figure 11 is a tabulation of the data plotted in Figure 10.

The three temperatures actually chosen for the test varied from test to test as the chamber had a great 'thermal inertia', and test controllers had great difficulty achieving a specified temperature in a reasonable time. The nominal temperatures are

close to 10°C, -25°C and -40°C. The temperature was measured by a thermistor on the PSA board. The actual gain values for the four flight cameras (FC-1B, FC-2A, FC-3A, Spare) and the other flight-qualified camera which didn't fly (FC-2B) are given in Figures 12-16. For plots of all data, tables of all raw data, and information about data tape numbers and file numbers, see the gain 'Calibration Data Transmittal Reports' for all cameras in Volume II of this report. Only representative raw data for a single camera (FC-1B) and final gain values for all cameras are presented here.

5.2 Offset Test

The offset test is outlined in Section 4.2. It must be remembered that the function of the offset is to "null out" any large D.C. signal to the amplifier input so as to prevent it from saturating. If this is done, small brightness variations in a high brightness area may be studied with the camera. Also, since the analog to digital converter in the camera does not correctly digitize small signals, the first two offset steps (numbered 0 and 1) are positive voltages, and the remainder are negative. This is done so that the A/D converter need never see small analog inputs: if the scene brightness is very low (such that the digitized value would be 5 or less), the camera can be commanded to use one of these positive offsets. If this is done, then the low scene brightness is added to the offset, thus avoiding the low signal area where improper A/D converter operation occurs.

During the offset test, the entire range of offsets (0→31) was exercised to monitor the effect on the camera output. At the lowest gain (= 5), a change of one offset step will change the camera output by 2 DN. If the camera is covered to exclude light and one picture is taken at each offset step, 32 pictures will result, each differing in its mean DN by 2 from the previous one. Also, there is considerable likelihood that the first or last picture will be saturated ($\overline{DN} < 0$ or $\overline{DN} > 63$). The low gain (= 5) introduces another problem, that of quantization error. We are looking at a 2 DN effect with a process which has a resolution of 1 DN. This problem can be lessened by using a higher gain. This is in fact what was done: a gain index of 3 was used throughout the test.

If a voltage V is applied to the "test connector" (see Fig. 1), the following equation applies:

$$DN = G(S + V + f) \tag{12}$$

If we exclude light from the camera, then S is zero, so we can solve for f:

$$f = \frac{DN}{G} - V \tag{13}$$

Since we used a gain index of 3 for the test (the actual gain value of index 3 is $\frac{1}{4}$ times that of index 5), one offset step change causes a change of 8 DN in the output. This meant that V had to

be changed every 6→8 offset steps, on the average, to avoid saturation. Thirty-two pictures were taken, one at each offset step, changing V when necessary to avoid saturation. Equation (13) was used to calculate the offset voltage for each step, from $\overline{DN}$ (the mean DN of the frame), V, and the gain. Figure 2 shows the result for FC-1B. As an example, let us take offset step 0 for FC-1B.

$$\overline{DN} = 56.007$$

$$V = 0.800 \text{ volts}$$

$$G = 55.781 \text{ DN/volt}$$

$$f_o = \frac{\overline{DN}}{G} - V = \frac{56.007}{55.781} - .8 = 0.204 \text{ volts} \qquad (14)$$

V was assumed to be correct only for the first few offset steps (first value of V). When V was changed, its value was <u>calculated</u> instead of being inferred from the actual voltage source setting. It was calculated by repeating the same offset step with both the old and new V values. The new V value was calculated from the following equation:

$$V_2 = V_1 + \left(\frac{DN_2 - DN_1}{G}\right) \qquad (15)$$

Then the offset values for the new value of V were again calculated from Eq. (14). Using Eq. (15) to calculate V_2 instead of believing the source settings eliminates any error of one source setting

relative to another. The source used was a digital voltage source, accurate to ±1/2 millivolt.

Figures 17 to 21 show the actual offset values determined for the cameras other than FC-1B, as determined from Eq. (14). Although a least squares line fitting process was used to find the slope of the offset step vs. voltage relationship, the numbers actually used in the calibration file are the ones determined point by point from Eq. (14), not the "smoothed" values. The actual raw data values and graphs of offset step vs. voltage appear in Volume II of this report. Figures 17 to 21 only relate the final results.

IPL requested that this test be run at three temperatures, in the same way the gain test was, but this was rejected by ITEK and VPO as too expensive. Hence, we only have results at one temperature ("room"). See Volume II of this report.

5.3 "Chalk Block" Absolute Calibration Test

This test is outlined in Section 4.3. Figure 22 shows the "Langley test fixture" which contained a calibrated lamp (Eppley S/N #1569) and a magnesium carbonate block. A system of baffles was used to reduce internal reflections. If the spectral irradiance of the lamp at 50 cm is W_λ μWATTS-CM^{-2}-NANOMETER^{-1}, then the spectral brightness or spectral radiance is:

$$S_\lambda = W_\lambda \cdot \left(\frac{\cos 20^\circ}{\pi}\right) \qquad (16)$$

Note that Equation (16) assumes that the spectral reflectivity of $MgCO_3$ is unity at all wavelengths and that its photometric function is Lambertian.

The cos 20° factor is required because the lamp is 20° off-axis (relative to the normal to the chalk block surface). Figure 23 is a table of the spectral radiance of the chalk block as illuminated by the lamp in the Langley test fixture.

The chalk block was imaged by all diodes (except SUN) and the mean DN of a 30x30 pixel patch centered on the block was computed. The "calibration constant" can then be computed from Eq. (17):

$$C = \frac{\int_0^\infty R_\lambda^* S_\lambda d\lambda}{\left(\frac{\overline{DN}}{G} - f\right)} \qquad (17)$$

where R_λ^* is the peak-normalized relative responsivity function for the entire optical system (i.e., window, mirror, lens, cover glass, PSA); S_λ is the spectral radiance of the source we calculated in Eq. (16); $\overline{DN}$ is the mean DN of the 30x30 pixel patch in the image of the chalk block, G is the gain used (see 5.1), and f is the offset used (see 5.2).

Since R_λ^* was measured at two temperatures by MMA, C can be calculated at two temperatures, provided images are taken at the same two temperatures. Unfortunately, taking images at other than room temperature required use of the ITEK thermo-vac chamber which

did not have a window in a position which would allow the camera to 'see out'. To remedy this, ITEK made a 'periscope' which consisted of two first-surface mirrors, arranged so that the camera could see out the chamber window. However, since data on window transmission and mirror reflectivity could never be obtained from ITEK, the test data in the thermal chamber was not reduced. For this reason the 'calibration constants' for different temperatures were calculated from PSA-level tests in a thermo-vac chamber at MMA. Two values of C were calculated for each diode. One value was obtained from Eq. (17) where DN was obtained at 20°C and R^*_λ was obtained at 20°C. The other value was obtained by correcting the 20°C value to -40°C by ratioing the peak values of the responsivity curves obtained by MMA at 20° and -40°C. This approach was suggested by the team engineer, William Patterson.

Since the IPL radiometric decalibration program, RADCAM, had been designed to use linear interpolation between three values of C, a third value was synthesized by linear interpolation between the two calculated values. Figures 24-28 are tables of the C values at three temperatures for all diodes (except SUN) for all cameras.

The SUN diode was not calibrated during the ITEK calibration tests, as a result of a lack of time and money. MMA did expose the SUN diode to the sun at Denver, and from this exercise a value of (milliamps/solar constant) was calculated for every flight PSA.

These data can be found in the PSA test documents published by MMA, which are listed at the end of this report.

5.4 Internal Calibration Test

This test is outlined in Section 4.7. There is a small lamp ('grain of wheat' bulb) located just above the PSA. It is possible to command the camera to turn on the light bulb and take three scan lines for each diode. In this manner, the response of each diode to a standard source is available. The bulb runs off a highly stable, regulated supply which has four commandable current levels. These are referred to as 'internal cal levels 0, 1, 2 and 3'. Only levels 2 and 3 produce useful output - level 0 is 'off', and level 1 is too low to be useful. Figures 29 and 30 are plots of the last scan line of the response of a RED diode (FC-2A) to internal cal levels 2 and 3, respectively. Note that the bulb is still coming up to full brightness at the end of the scan for internal cal level 2, and that even for internal cal level 3, one must use only the last 100 digitized values (samples) or so to be sure that the bulb has reached full brightness.

Figure 31 shows the mean DN for the last 100 samples of the third scan line for all diodes, camera FC-1B. This test was run at 10°C, -25°C and -40°C for all cameras. The tables of all these data for all flight cameras appears in Volume II of this report.

5.5 Camera Response as a Function of Elevation Angle

This test is outlined in Section 4.8.

There was concern among the imaging team that the sensitivity of the camera might depend on the elevation angle that the camera was viewing. For reasons of limited time and money, it was possible to set up only a very restricted test for this, utilizing a flat-field diffuse source. We mounted the camera in the 'swing fixture'; a device capable of holding the camera and tilting it accurately to any angle in 10° increments in elevation. In this fashion, the camera was able to look at the source at any desired elevation angle, without having to move the source up or down. We were only able to get enough test time to do the test at four elevation angles, viz., -50°, -30°, 0°, +30°. The test was done twice: once with the contamination cover open and once again with it closed.

Figures 35 and 36 show the resulting DN in the image of the source as a function of elevation angle, contamination cover open. Note that any effect is less than 1 DN in magnitude. In contrast with this, see Figures 32 and 33. They are the result of the same test, but with the contamination cover closed. Figure 34 is the table of data plotted in Figures 32 and 33. Note that the drop in DN is considerable with the cover closed at +30°. (Since straight lines were drawn to connect the points in Figures 32 and 33, one might gain the mistaken impression that the onset of the vignetting

is 0°. Actually, the onset is at approximately 25^{o}.) Also note that the drop in DN for blue, green and red is related as follows: blue>green>red. In other words, the blue diode experienced the greatest drop in DN. Similarly, the drops in DN for the infrared diodes are related as follows: IR3>IR2>IR1. Furthermore, the ratio of BLUE (closed) to BLUE (open) is almost exactly equal to the ratio IR3 (closed) to IR3 (open). The same is true for the pair GREEN/IR2 and RED/IR1. Figure 37 is a schematic of the diode placement on the PSA. From this we can deduce that the drop in sensitivity at +30" is a function of distance from the end of the PSA, not of diode center wavelength.

If we extrapolate this idea, we predict that the BB1 and BB2 diodes should show the greatest effect. A later test on the Science Test Lander indeed verified this. With the cover closed, the camera simply could not 'see' anything above roughly +30° in elevation with the BB1 and BB2 diodes. However, the BB3 and BB4 diodes (at the opposite end of the PSA) showed no less of sensitivity, at any elevation angle.

All this strongly suggests a vignetting effect instead of a wavelength dependent transmission effect. From a knowledge of internal camera geometry, one can conclude that the small metal frame on the contamination cover is the cause of the problem. A more thorough test was run on the FC-1A camera on the Science Test Lander in October, 1976. Figures 38 through 43 are plots of the

ratio of closed to open transmission through the contamination cover, as a function of elevation. Since the window transmits only about 93% of the light, the plots have been corrected for this. This was done by multiplying the ratio by a number so that it comes out 1.0 at 0°. Also, one must correct for the electronic offset in the camera. If the 'background DN' in the image taken with the cover closed is DN_c, and the 'background DN' in the image taken with the cover open is DN_o, then the following formula can be used to obtain the vignetting ratio:

$$R = \frac{(DN_c - F_c)}{(DN_o - F_o)} \cdot Q \qquad (18)$$

where Q is a factor needed to make R come out 1.0 at 0° elevation. Q will be different for different diodes, and will be numerically equal to 1/T, where T is the transmission of the window at the wavelength of the diode in question.

The original test report on the limited tests taken on all cameras at ITEK is reproduced in Volume II of this report. Tables of the vignetting ratio, R, for all diodes of camera FC-1A are also in Volume II of this report.

5.6 Coherent Noise Test

This test is outlined in Section 4.11.

Throughout this test the room lights were turned out and a heavy black cloth was placed over the camera. Short frames

(approximate 100→125 scan lines) were taken with each diode, first with the dark current subtractor on and again with it off. The test was done at room temperature, and then the BB2 diode part was repeated at -40°C and -25°C. Also, the low data rate mode was used for diodes BB1 and SURVEY to see if any unique coherent noise problems existed in that mode (that is in addition to the frames taken with BB1 and SURVEY in high data rate). This test plan was adhered to except in the case of camera FC-1B, where the low temperature part was omitted.

Data analysis consisted of taking the Fourier transform of each and every scan line and then averaging them (root-mean-square) and plotting the result. The vertical axis of the plots is in peak-to-peak DN, and the horizontal one in cycles per sample (or cycles per pixel). In this frequency scale, the maximum frequency one can expect is one cycle in two pixels (alternating high, low, high, low, . . .), hence the maximum value is 0.5 CPS (Cycles Per Sample). To convert this to Hertz, one must multiply by the encoding rate of the camera (3200 samples per second in high data rate). Hence, the maximum on this scale also represents 1600 HZ.

Figure 44 shows a typical power spectrum plot (actually for the green diode, FC-1B). Note the peaks at 0.16, 0.26 and 0.37 CPS. Figure 45 is the image that the plot represents. Note the coherent noise bars in the image.

In low data rate, the sampling rate is so low that most coherent noise frequencies are 'aliased' into D.C. or pure random noise, hence they seem to disappear. See Figures 46 and 47 which are from BBl diode, FC-2A camera, same gain. The first plot is at high data rate and the second at low data rate.

Another coherent noise effect is demonstrated by Figure 4. It is sometimes called the 'venetian blind effect', for obvious reasons. It is caused by a drifting integrator I.C. in the camera dark current subtractor circuit. This image was taken with the Science Test Camera. It is less of a problem at low gain and low temperatures.

As a result of IPL's intense analysis of coherent noise, particularly in the so-called Science Test Camera (STC), ITEK found a problem in the camera design. A tuning stub on one circuit board was microphonic (resonating with camera mechanical vibrations). Due to the precise nature of the noise peak in IPL Fourier transform plots (low Q, not very coherent, frequency varying, high amplitude), ITEK engineers were able to isolate and fix the problem. The 'fix' consisted of epoxying the stub firmly in place so it could not vibrate. This 'fix' was retrofitted to all flight units. This is the reason that they are so quiet compared to STC. See Figure 48 for an example of this problem before the fix.

Volume II of this report contains all the power spectrum plots for all flight cameras.

5.7 Point Spread Function Test

This test is outlined in Section 4.12.

It consisted of the camera imaging a sub-pixel diameter pinhole, backlit. Two images were taken with each diode: one at a gain which did not saturate the 'peak' and other at a gain four times as great. Although the 'point spread function' so obtained is obviously undersampled, and thus not truly representative of the camera MTF, the test was retained to flight level testing to check for any gross problems such as internal reflections, light leaks from aperture to aperture, etc.

The only anomalies observed were with the BB3 diode, FC-3A camera and with the GREEN diode, FC-2B camera. FC-2B did not 'fly', but FC-3A did. Figures 49 and 50 are pixel listings of BB3 images, FC-3A camera. The first is the 'primary' peak in the image of the pinhole, the second is the 'secondary' peak. The relative orientation of the secondary peak relative to the primary one (.96° lower in elevation, same azimuth) strongly suggests that the cause is a leak from the SURVEY diode aperture. In other words, light passing through the SURVEY diode aperture is not being fully blocked by the PSA internal baffle and is finding its way over to the BB3 diode (see Figure 37 which is a schematic diagram of the PSA diode placement). The ratio of the peaks is 159:1 (after correcting for offset), so it is not really a serious problem.

Another secondary peak was observed with the GREEN diode, in the FC-2B camera (see Figure 51). This peak was about 0.96 degrees away from the primary one in azimuth, and at the same elevation. This strongly suggests that the leak is from the IR2 diode, which is just 0.96° away in azimuth. The intensity ratio of the peaks is 88:1, after correcting for offset.

Point spread function listings for all diodes are presented in Volume II of this report.

6. RADIOMETRY ERROR ANALYSIS

The 'diode lumens' corresponding to a given DN value in a Viking Lander camera image taken with a given gain, G, and a given offset, f, is:

$$L = C^k \left(\frac{DN}{G} - f \right) \tag{19}$$

where C^k is the appropriate calibration constant for the k^{th} diode. The change in L resulting from incremental changes (errors) in C^k, DN, G and f is just:

$$\Delta L = \frac{\partial L}{\partial C^k} \cdot \Delta C^k + \frac{\partial L}{\partial DN} \cdot \Delta DN + \frac{\partial L}{\partial G} \cdot \Delta G + \frac{\partial L}{\partial f} \cdot \Delta f \tag{20}$$

The appropriate partial derivatives are easy to determine by inspection:

$$\frac{\partial L}{\partial C^k} = \left(\frac{DN}{G} - f\right) \tag{21}$$

$$\frac{\partial L}{\partial DN} = \frac{C^k}{G} \tag{22}$$

$$\frac{\partial L}{\partial G} = - \frac{DN \cdot C^k}{G^2} \tag{23}$$

$$\frac{\partial L}{\partial f} = - C^k \tag{24}$$

We must now supply reasonable values for ΔC^k, ΔDN, ΔG and Δf so Eq. (20) can be evaluated. In the following analysis, a typical case will be assumed (BB2 diode, FC-2A). However, the general approach is outlined so that the reader can calculate the uncertainty in 'diode lumens' for any channel, any camera.

6.1 Uncertainties in DN

Uncertainties in DN arise from four sources:

1) coherent noise

2) incoherent ('white') noise

3) dark current subtractor drift

4) quantization noise

Totalling up the peak-to-peak coherent noise amplitudes for BB2, FC-2A we get 7.0 DN peak-to-peak. The incoherent noise level is about 0.2 DN (the baseline of the power spectrum plot). Dark current subtractor noise is about 4 DN at a gain of 0 (highest gain). Reducing all these gain-dependent effects to the same gain value and then reducing the result to a gain of 4, we get a value of 1.15 DN. To this we must add the quantization noise, ±0.5 DN. The result is ±1.65 DN at a gain of 4 (4 is the most commonly used gain).

6.2 Uncertainties in Gain

Gain values were determined by the slope of a DN versus voltage plot. DN values were determined as the average over a 30x30 pixel area. This would tend to greatly reduce both the incoherent and coherent noise, probably to the point where they can be ignored. We are left with quantization noise and voltage source error (±1/2 millivolt). In the worst case, the endpoints of the straight line plot would be off 1/2 DN in opposite directions, and 1/2 millivolt in opposite directions. For FC-2A, gain 4, this would give a gain 2% different than actually obtained. Thus, ΔG is 27.6 x .02 = 0.55.

6.3 Uncertainties in Offset

The offset error is primarily from the D.C. source error (1/2 millivolt) and the gain uncertainty. If we assume 2% gain uncertainty in the offset calculations (see Section 5.2), then we

get a ±17 millivolt uncertainty in offset, independent of the step number. The ±1/2 millivolt uncertainty in the voltage source should be added to this, but this is really negligible. Hence, $\Delta f = 0.017$.

6.4 Uncertainty in Calibration Constant

As we recall from Section 5.3, the calibration constant is calculated from the following equation:

$$C = \frac{\int_0^\infty R_\lambda^* S_\lambda \, d\lambda}{\frac{DN}{G} - f} \qquad 17$$

If we assume an uncertainty of ±5% for the PSA responsivity curves (R_λ^*) generated at MMA, and ±3.2% uncertainty in the standard lamp radiance function (S_λ), we can then use the uncertainties we have already calculated for DN, G and f to derive an uncertainty for C. When we do this, we ±11.8% for BB2 diode, FC-2A camera. Hence, $\Delta C = 0.118 = 1056 \times 0.118 = 125$.

6.5 Uncertainty in L

Plugging in Eq. (20), we can now calculate the total uncertainty in L for a special case. Let's assume BB2 diode, FC-2A camera, offset = 1, gain = 4, DN = 32 (on a six-bit scale). The resulting ΔL is ±21%. If we combine the terms of Eq. (20) by RSS instead of summing, the total uncertainty in L is ±13%.

This is as realistic an estimate as we can really come up with for our uncertainty in the 'diode lumens' calculations done by program RADCAM.

BIBLIOGRAPHY

ALLEN, C. W., Astrophysical Quantities, Oxford University Press, 1964.

HUCK, F.O., Et. Al., "Radiometric Performance of the Viking Mars Lander Cameras", NASA TM X-72692, 1975.

Martin Marietta Document #MCR 74-038 "Acceptance Test Report for Photo Sensor Array Unit #15."

Martin Marietta Document #MCR 74-034 "Acceptance Test Report for Photo Sensor Array Unit #17."

Martin Marietta Document #MCR 74-035 "Acceptance Test Report for Photo Sensor Array Unit #19."

Martin Marietta Document #MCR 74-036 "Acceptance Test Report for Photo Sensor Array Unit #20."

WALL, S.D., Et. Al., "Reflectance Characteristics of the Viking Lander Reference Test Charts", NASA TM X-72762, 1975.

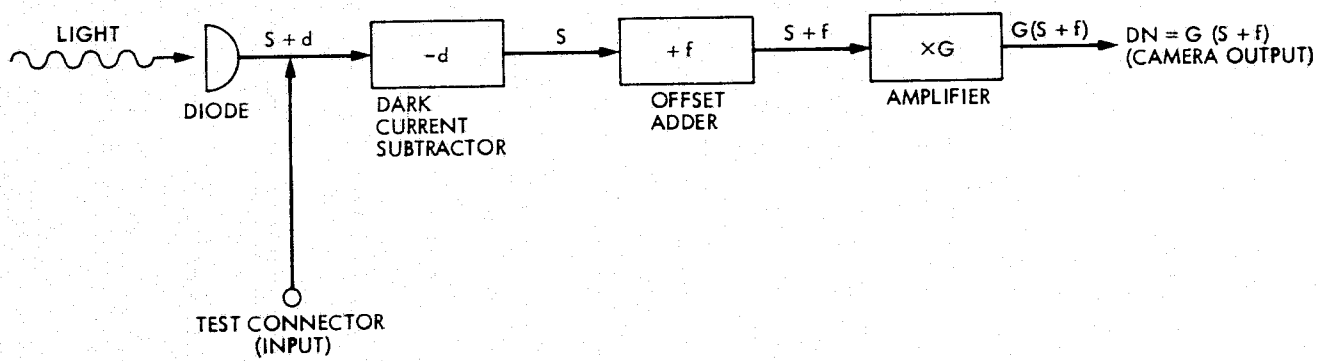

Figure 1. Viking Lander Camera Radiometric Model

Offset Number	DN Values	Offset, Volts
0	56.007	0.204053
1	48.000	0.060510
2	40.037	0.082245
3	32.000	-0.226327
4	24.000	-0.389745
5	16.000	-0.513163
5	55.000	-0.513163
6	47.000	-0.656581
7	38.999	-0.800017
8	31.000	-0.943418
9	23.001	-1.086818
10	15.000	-1.230254
10	54.000	-1.230253
11	46.000	-1.373672
12	38.000	-1.517090
13	30.000	-1.660508
14	22.000	-1.803926
15	14.000	-1.947345
15	53.000	-1.947344
16	45.000	-2.090762
17	37.000	-2.234180
18	28.968	-2.378173
19	21.000	-2.521017
20	13.000	-2.664435
20	52.000	-2.664434
21	44.000	-2.807853
22	36.000	-2.951271
23	27.998	-3.094726
24	19.483	-3.247376
25	11.000	-3.399453
25	56.000	-3.399454
26	48.000	-3.542871
27	39.999	-3.686308
28	31.961	-3.830407
29	23.920	-3.974560
30	15.771	-4.120649
31	7.811	-4.263350

Figure 2. FC-1B Offset Values

Gain Setting	Gain/Temp	Gain/Temp	Gain/Temp
0	452.870261/+10°C	433.331787/-27°C	419.773682/-41°C
1	224.776306/+10°C	223.400360/-27°C	224.349548/-41°C
2	111.911591/+10°C	112.620056/-27°C	110.675858/-41°C
3	55.577942/+10°C	55.647614/-27°C	55.507950/-41°C
4	27.388290/+10°C	27.496718/-29°C	27.356552/-41°C
5	13.790790/+8°C	13.724940/-29°C	13.734254/-43°C

Figure 3. FC-1B Gain Values

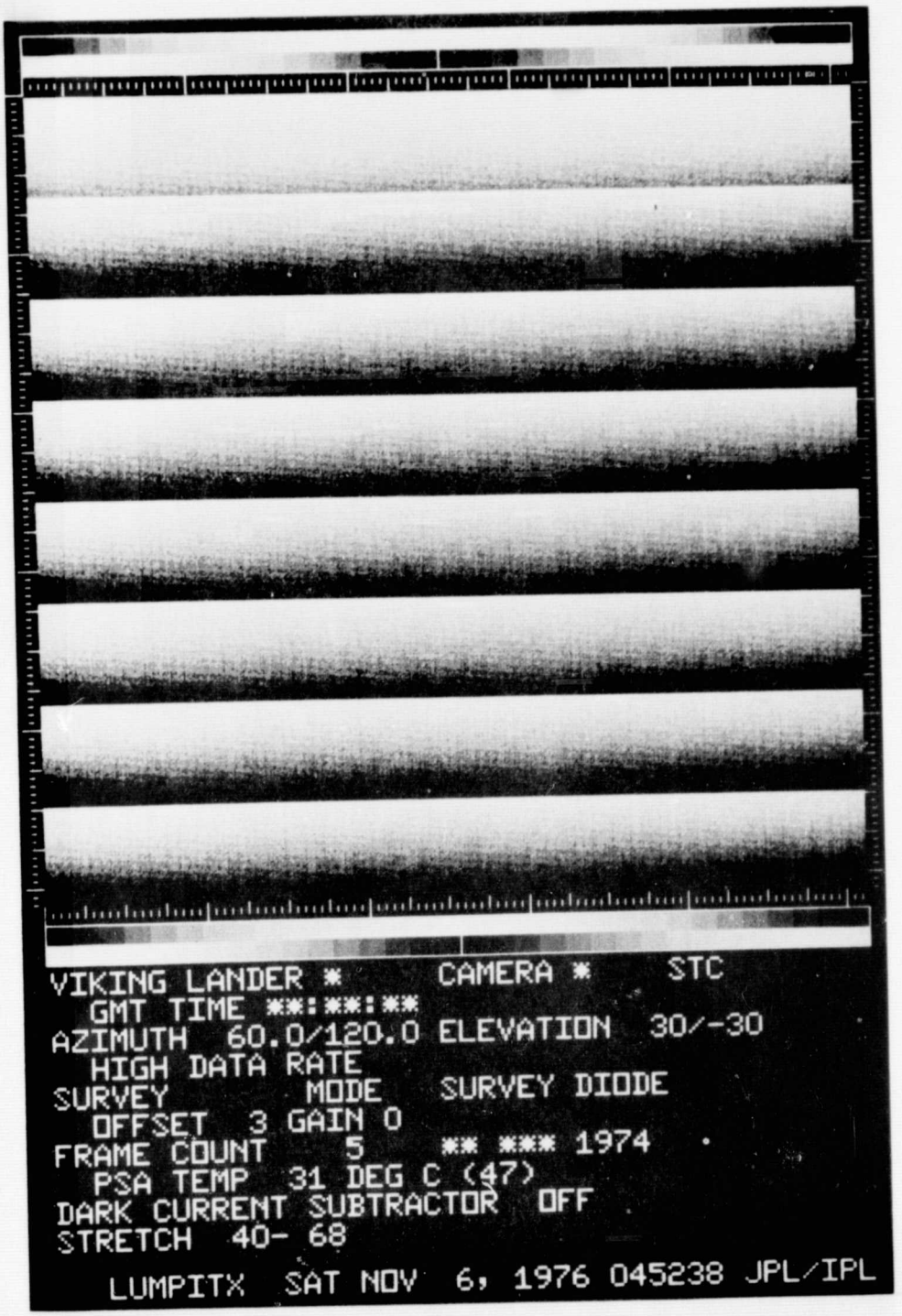

Figure 4. Dark Current Subtractor Effect — High Data Rate

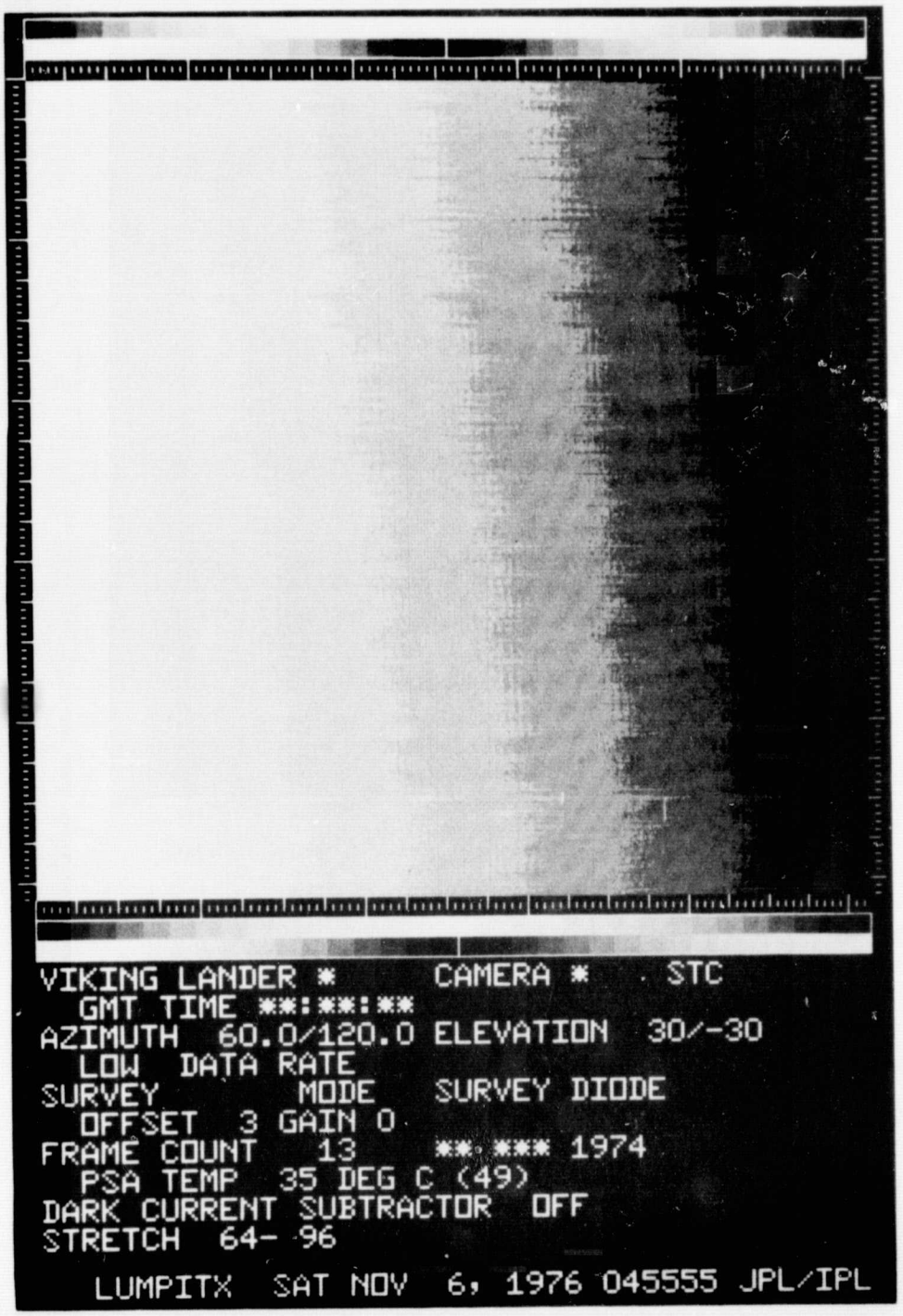

Figure 5. Dark Current Subtractor Effect — Low Data Rate

λ, nm	Irradiance, μW/cm²-nm
320	0.366
350	0.826
370	1.28
400	2.23
450	4.48
500	7.52
550	11.0
600	14.6
650	18.0
700	20.9
750	23.2
800	24.7
900	25.5
1000	24.8
1100	23.5
1200	21.7
1300	19.7

Figure 6. Spectral Distribution of Lamp EPI-1569 (Spectral Irradiance at 50 cm as a Function of Wavelength)

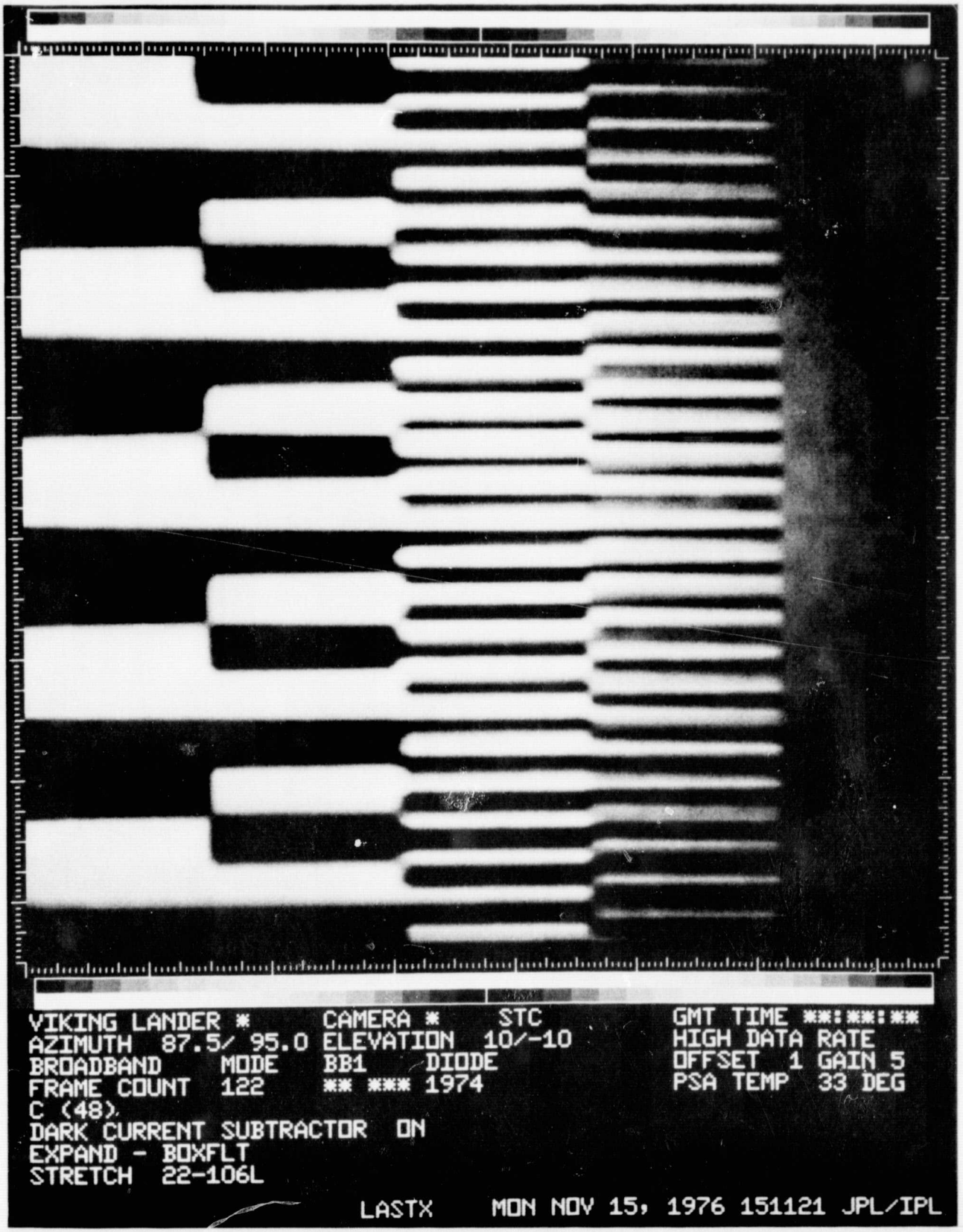

Figure 7. Square Wave Target Showing Source Vignetting

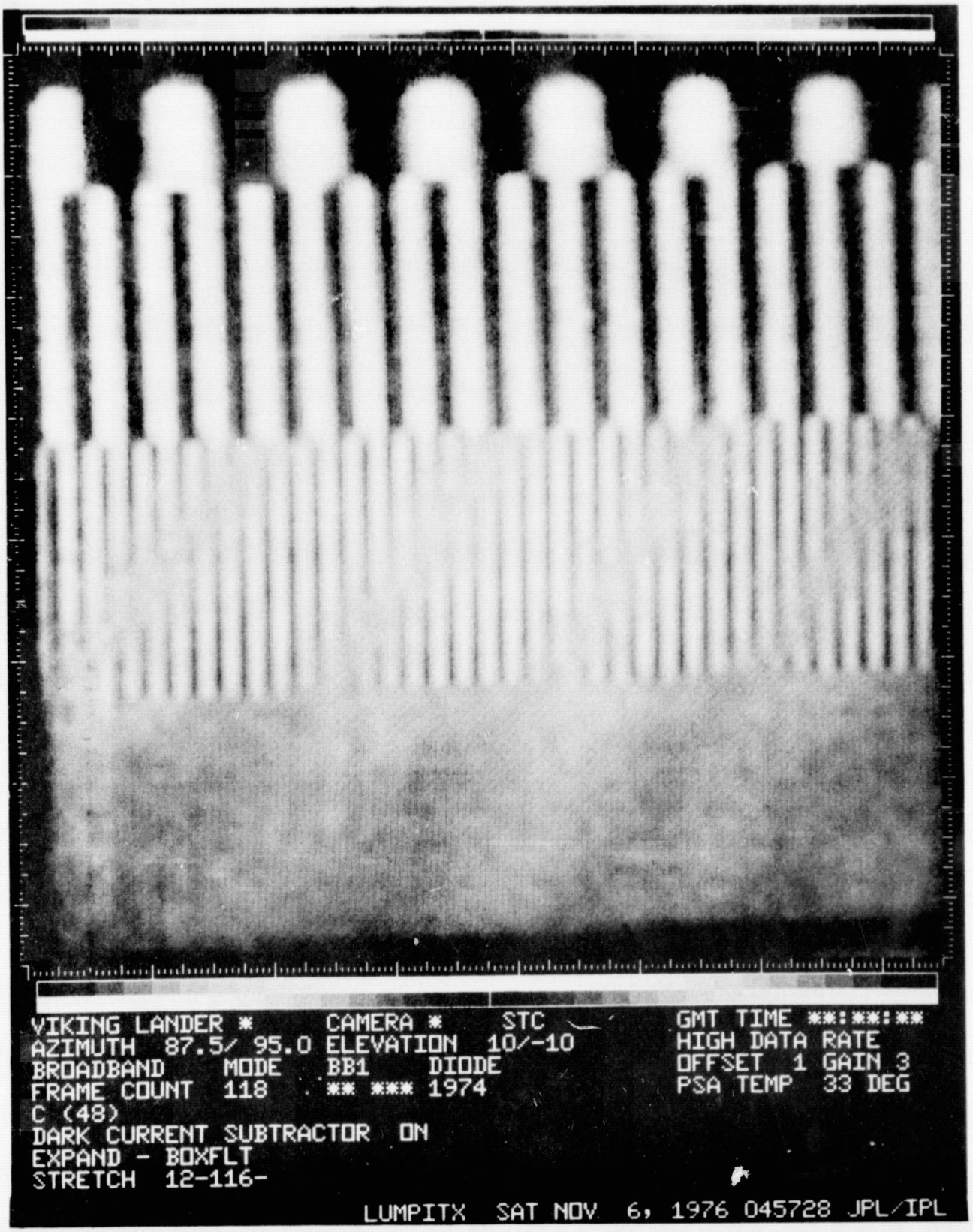

Figure 7A. Sinewave Target

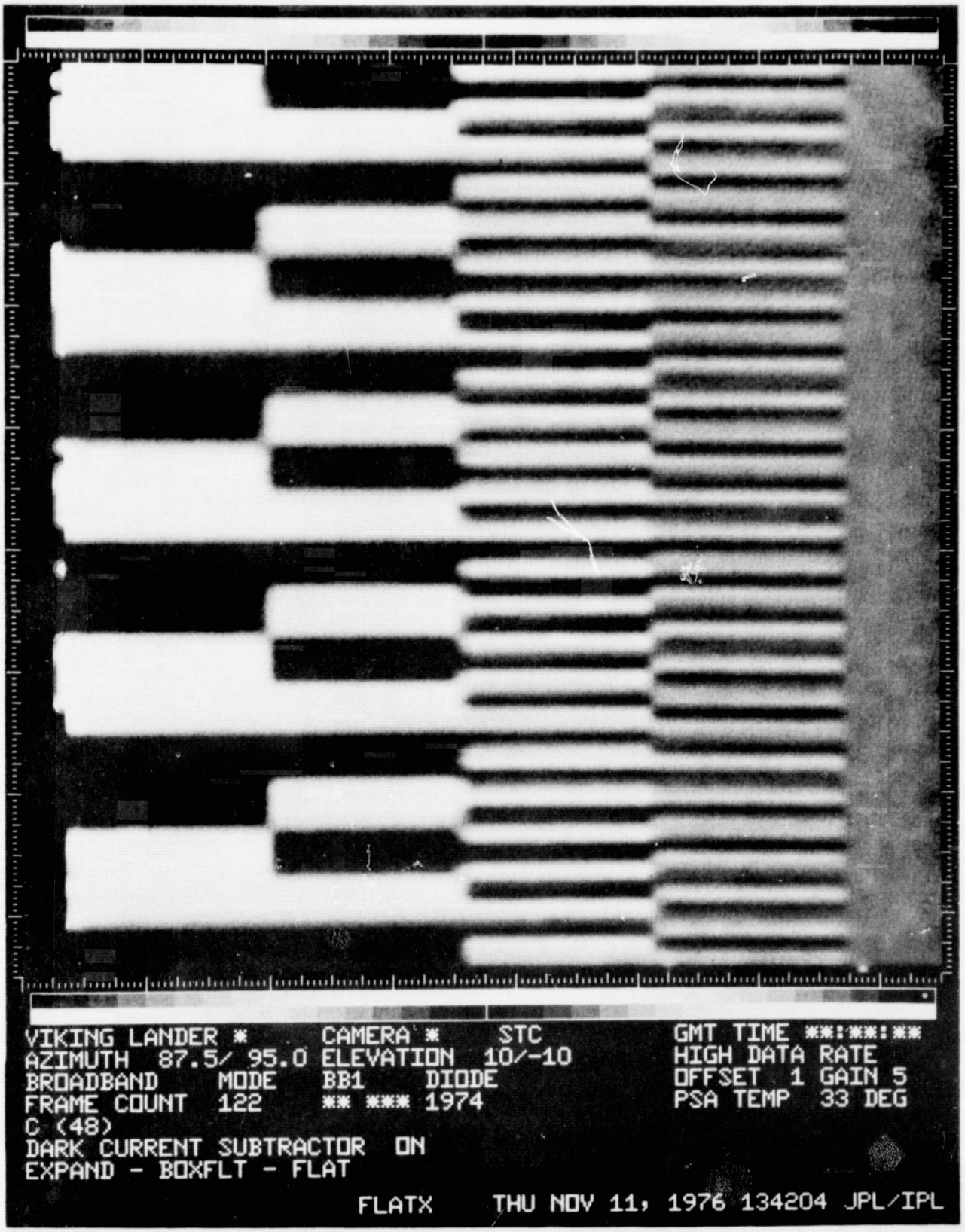

Figure 8. Square Wave Target — Vignetting Rectified

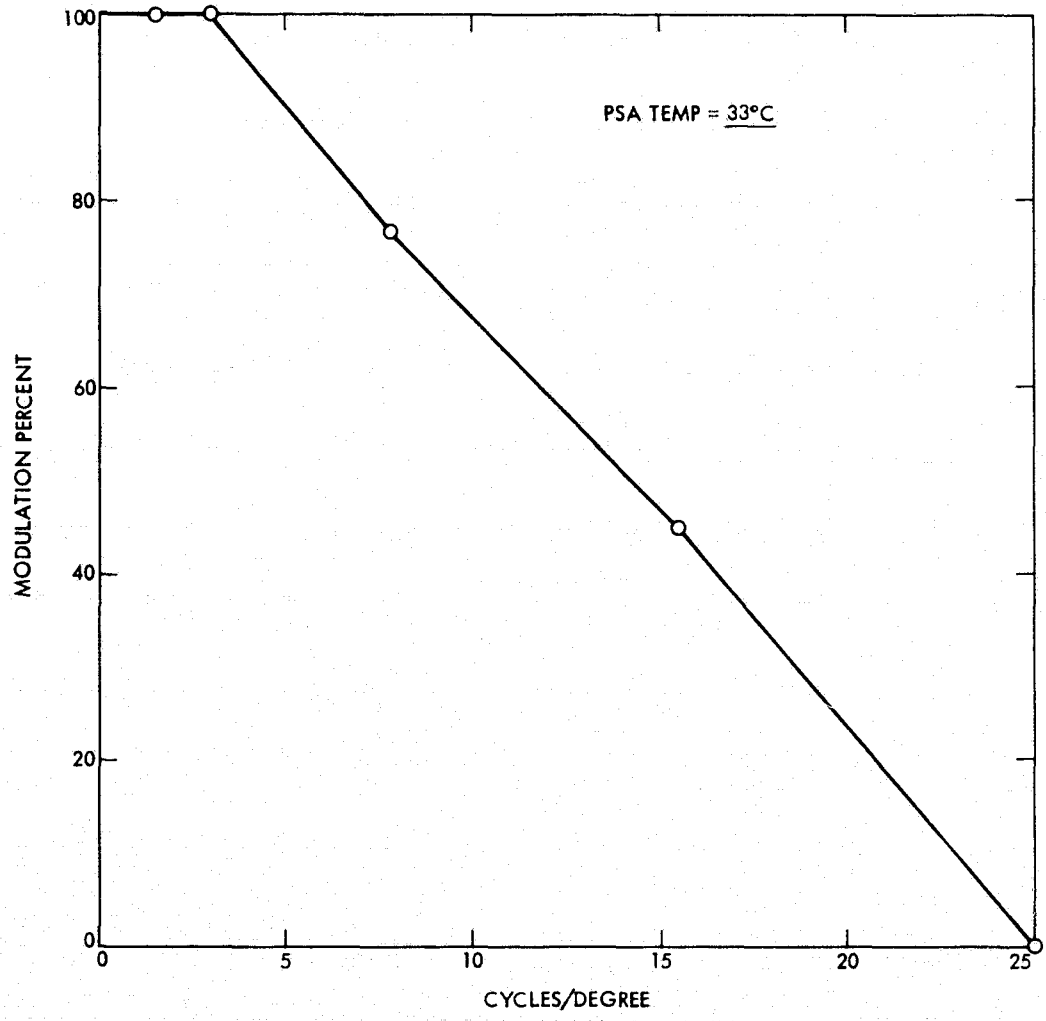

Figure 9. Bar Target MTF BB1 Diode STC Camera (Best Focal Distance) Bars Perpendicular to Scan

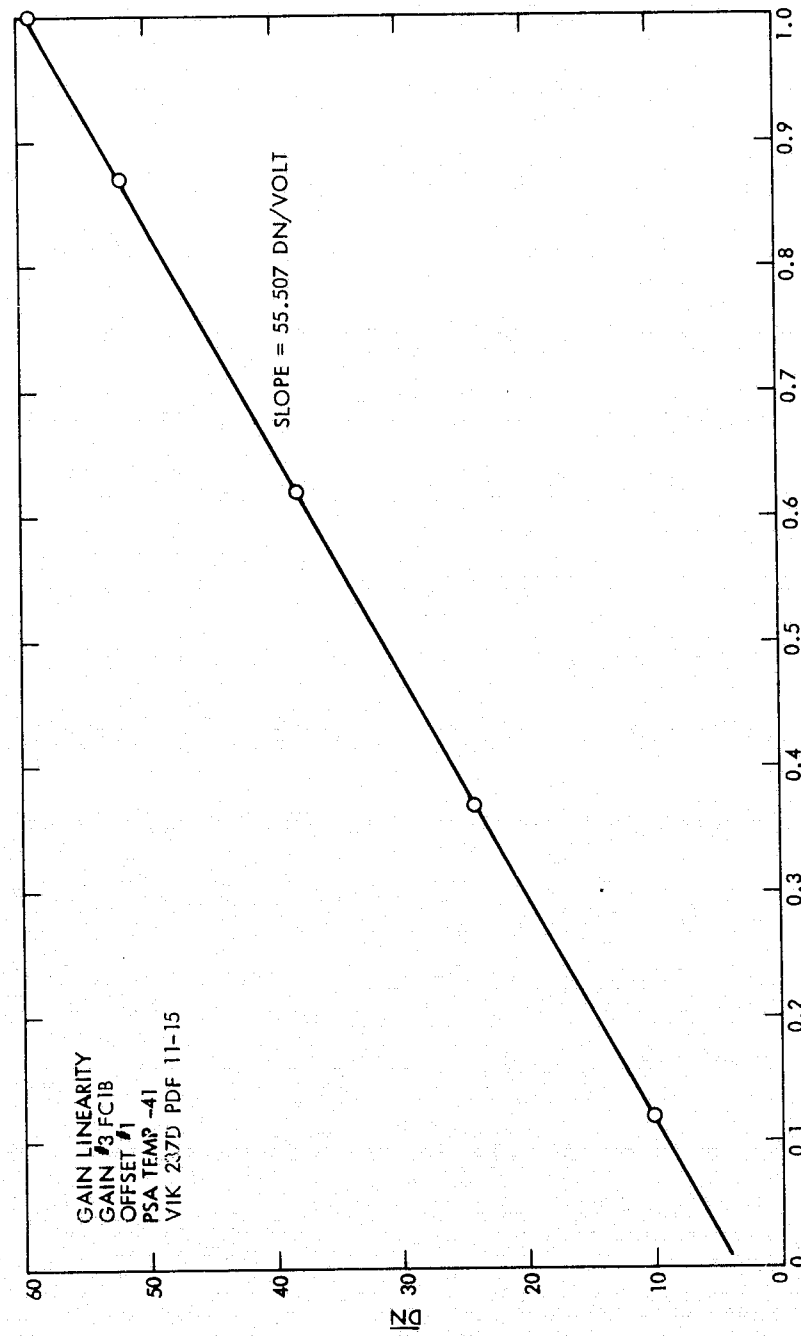

Figure 10. Gain Linearity FC-1B

Tape: VIK237D		Files: 11-15	
Gain: 3		Offset: 1	
PSA Temp: -41°C		Survey Diode Select	
Volts	DN	±	Sigma
1.00	59.049		0.240
0.87	52.000		0.0
0.62	38.118		0.325
0.37	24.090		0.287
0.12	10.301		0.459

Figure 11. FC-1B Thermal Calibration Test — Gain Linearity

Gain Setting	Gain/Temp	Gain/Temp	Gain/Temp
0	452.870261/+10°C	433.331787/-27°C	419.773682/-41°C
1	224.776306/+10°C	223.400360/-27°C	224.349548/-41°C
2	111.911591/+10°C	112.620056/-27°C	110.675858/-41°C
3	55.577942/+10°C	55.647614/-27°C	55.507950/-41°C
4	27.388290/+10°C	27.496718/-29°C	27.356552/-41°C
5	13.790790/+8°C	13.724940/-29°C	13.734254/-43°C

Figure 12. FC-1B Gain Values

Gain Setting	Gain/Temp	Gain/Temp	Gain/Temp
0	405.01196/+14°C	436.30615/-23°C	336.75488/-39°C
1	221.38408/+14°C	221.37360/-23°C	217.60587/-39°C
2	110.87958/+12°C	109.38438/-25°C	110.68680/-39°C
3	55.49237/+10°C	55.33073/-25°C	55.77348/-39°C
4	27.63736/+10°C	27.49220/-27°C	27.32755/-39°C
5	13.71505/+10°C	13.71571/-27°C	13.72112/-41°C

Figure 13. FC-2A Gain Values

Gain Setting	Gain/Temp	Gain/Temp	Gain/Temp
0	460.9187/-39°C	413.3191/-27°C	467.9094/+12°C
1	225.2655/-39°C	225.0350/-27°C	224.7278/+12°C
2	111.3538/-41°C	111.1463/-29°C	111.2316/+12°C
3	55.4826/-41°C	55.7809/-29°C	55.7809/+12°C
4	27.9999/-41°C	27.9999/-29°C	27.9999/+10°C
5	14.0397/-41°C	14.0397/-31°C	14.0397/+10°C

Figure 14. FC-3A Gain Values

Gain Setting	Gain/Temp	Gain/Temp	Gain/Temp
0	450.55420/+16°C	404.18408/-27°C	451.39233/-39°C
1	228.76236/+14°C	220.27850/-27°C	223.72998/-39°C
2	111.45090/+14°C	112.71609/-27°C	111.56445/-39°C
3	55.78564/+14°C	55.76968/-27°C	55.78088/-39°C
4	27.99994/+14°C	27.99994/-29°C	27.31877/-39°C
5	13.84129/+14°C	13.84129/-29°C	13.71861/-39°C

Figure 15. Spare Gain Values

Gain Setting	Gain/Temp	Gain/Temp	Gain/Temp
0	428.5955/+12°C	471.0098/-27°C	455.7153/-39°C
1	225.2572/+12°C	222.8364/-27°C	222.8007/-39°C
2	112.0243/+12°C	110.9847/-29°C	110.5197/-41°C
3	55.9039/+10°C	55.7810/-29°C	55.7810/-41°C
4	27.9945/+10°C	27.4971/-29°C	27.3980/-41°C
5	13.7284/+10°C	13.8009/-31°C	13.7211/-41°C

Figure 16. FC-2B Gain Values

Offset Number	DN Values	Offset, Volts
0	56.007	0.204053
1	48.000	0.060510
2	40.037	0.082245
3	32.000	-0.226327
4	24.000	-0.389745
5	16.000	-0.513163
5	55.000	-0.513163
6	47.000	-0.656581
7	38.999	-0.800017
8	31.000	-0.943418
9	23.001	-1.086818
10	15.000	-1.230254
10	54.000	-1.230253
11	46.000	-1.373672
12	38.000	-1.517090
13	30.000	-1.660508
14	22.000	-1.803926
15	14.000	-1.947345
15	53.000	-1.947344
16	45.000	-2.090762
17	37.000	-2.234180
18	28.968	-2.378173
19	21.000	-2.521017
20	13.000	-2.664435
20	52.000	-2.664434
21	44.000	-2.807853
22	36.000	-2.951271
23	27.998	-3.094726
24	19.483	-3.247376
25	11.000	-3.399453
25	56.000	-3.399454
26	48.000	-3.542871
27	39.999	-3.686308
28	31.961	-3.830407
29	23.920	-3.974560
30	15.771	-4.120649
31	7.811	-4.263350

Figure 17. FC-1B Offset Values

Offset Number	DN Values	Offset, Volts
0	56.000	0.20915
1	48.000	0.06498
2	40.000	-0.07918
3	32.000	-0.22334
4	24.001	-0.36749
5	16.000	-0.51167
5	55.000	-0.51167
6	47.000	-0.65584
7	39.000	-0.00000
8	31.000	-0.94416
9	23.000	-1.08833
10	15.000	-1.23249
10	54.000	-1.23249
11	46.000	-1.37665
12	38.000	-1.52082
13	30.000	-1.66498
14	22.000	-1.80915
15	14.000	-1.95331
15	52.999	-1.95331
16	45.000	-2.09746
17	36.998	-2.24166
18	28.531	-2.39424
19	20.999	-2.52997
20	12.586	-2.66157
20	51.000	-2.68157
21	43.059	-2.82467
22	35.001	-2.96988
23	27.044	-3.11327
24	19.112	-3.25621
25	11.012	-3.40217
25	36.000	-3.40217
26	48.000	-3.54634
27	40.000	-3.69058
28	31.888	-3.83668
29	23.924	-3.90020
30	15.049	-4.14013
31	7.000	-4.28518

Figure 18. FC-2A Offset Values

Offset Number	DN Values	Offset, Volts
0	57.000	0.221855
1	49.000	0.078437
2	40.996	-0.065053
3	32.906	-0.210085
4	24.000	-0.369745
5	16.000	-0.513163
5	55.999	-0.513164
6	47.456	-0.666316
7	39.000	-0.817908
8	31.784	-0.947272
9	23.002	-1.104709
10	15.663	-1.236278
10	55.000	-1.236277
11	46.997	-1.379749
12	38.878	-1.525301
13	30.147	-1.681824
14	22.000	-1.827877
15	14.000	-1.971295
15	53.960	-1.971294
16	45.443	-2.123981
17	37.019	-2.275001
18	29.000	-2.418759
19	21.000	-2.562178
20	13.000	-2.705596
20	52.000	-2.705595
21	44.000	-2.849013
22	36.000	-2.992432
23	28.000	-3.135850
24	20.000	-3.279268
25	12.000	-3.422687
25	57.000	-3.422687
26	49.000	-3.566104
27	40.999	-3.709541
28	32.332	-3.864917
29	24.073	-4.012978
30	16.001	-4.157687
31	8.000	-4.301124

Figure 19. FC-3A Offset Values

Offset Number	DN Values	Offset, Volts
0	56.738	0.21707
1	48.501	0.06942
2	40.439	-0.07510
3	32.001	-0.22636
4	24.006	-0.36967
5	16.000	-0.51319
5	55.012	-0.51319
6	47.071	-0.65554
7	39.000	-0.80021
8	31.564	-0.93351
9	24.000	-1.06910
10	15.993	-1.21263
10	54.833	-1.21263
11	46.996	-1.35312
12	38.348	-1.50814
13	30.831	-1.64289
14	22.477	-1.79264
15	14.692	-1.93219
15	53.999	-1.93219
16	45.997	-2.07563
17	37.000	-2.23691
18	29.468	-2.37193
19	21.666	-2.51178
20	13.000	-2.66713
20	52.057	-2.66713
21	44.019	-2.81121
22	36.101	-2.95315
23	28.002	-3.09833
24	20.000	-3.24177
25	12.000	-3.38518
25	57.000	-3.38518
26	49.000	-3.52858
27	41.000	-3.67199
28	33.000	-3.81540
29	25.000	-3.95880
30	16.997	-4.10226
31	8.998	-4.24565

Figure 20. Spare Offset Values

Offset Number	DN Values	Offset, Volts
0	56.007	0.201844
1	48.000	0.058617
2	40.037	-0.083824
3	32.000	-0.227589
4	24.000	-0.370691
5	16.000	-0.513794
5	55.000	-0.513793
6	47.000	-0.656896
7	38.999	-0.800017
8	31.000	-0.943102
9	23.001	-1.086186
10	15.000	-1.229307
10	54.000	-1.229307
11	46.000	-1.372410
12	38.000	-1.515512
13	30.000	-1.658615
14	22.000	-1.801719
15	14.000	-1.944821
15	53.000	-1.944821
16	45.000	-2.087924
17	37.000	-2.231027
18	28.968	-2.374702
19	21.000	-2.517232
20	13.000	-2.660335
20	52.000	-2.660335
21	44.000	-2.803437
22	36.000	-2.946541
23	27.998	-3.089680
24	19.483	-3.241995
25	11.000	-3.393737
25	56.000	-3.393737
26	48.000	-3.536839
27	39.999	-3.679959
28	31.961	-3.823743
29	23.920	-3.967579
30	15.771	-4.113347
31	7.811	-4.255733

Figure 21. FC-2B Offset Values

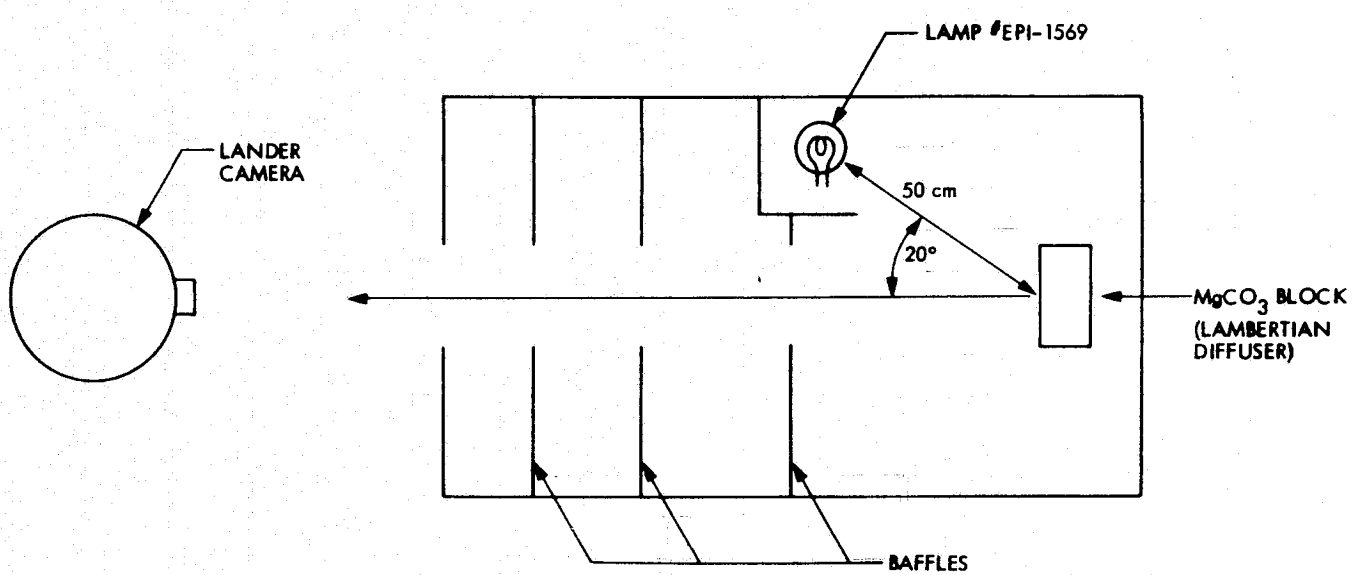

Figure 22. Langley Test Fixture, Approximate Schematic (Plan View)

λ, nm	Radiance, $\mu W/cm^2$-sr-nm
320	0.117
350	0.263
370	0.407
400	0.710
450	1.43
500	2.39
550	3.50
600	4.65
650	5.73
700	6.65
750	7.38
800	7.86
900	8.12
1000	7.89
1100	7.48
1200	6.91
1300	6.27

Figure 23. Spectral Distribution of Light Reflected From Chalk Block in Langley Test Fixture

Contamination Cover Out of Optical Path

Diode	Value 1	Temp 1	Value 2	Temp 2	Value 3	Temp 3
BB-2	1040.300	30	1040.300	30	1040.300	30
Blue	124.100	30	124.100	30	124.100	30
Green	114.500	30	114.500	30	114.500	30
Red	284.600	30	284.600	30	284.600	30
Sun	10000.001	30	10000.000	30	10000.001	30
BB-4	1047.800	30	1047.800	30	1047.800	30
BB-1	1040.300	30	1040.300	30	1040.300	30
IR-3	148.080	30	148.080	30	148.080	30
IR-2	116.280	30	116.280	30	116.280	30
IR-1	172.460	30	172.460	30	172.460	30
BB-3	1086.100	30	1086.100	30	1086.100	30
Survey	965.440	30	965.440	30	965.440	30

Contamination Cover Within Optical Path

Diode	Value 1	Temp 1	Value 2	Temp 2	Value 3	Temp 3
BB-2	1040.300	30	1040.300	30	1040.300	30
Blue	124.100	30	124.100	30	124.100	30
Green	114.500	30	114.500	30	114.500	30
Red	284.600	30	284.600	30	284.600	30
Sun	10000.001	30	10000.000	30	10000.001	30
BB-4	1047.800	30	1047.800	30	1047.800	30
BB-1	1040.300	30	1040.300	30	1040.300	30
IR-3	148.080	30	148.080	30	148.080	30
IR-2	116.280	30	116.280	30	116.280	30
IR-1	172.460	30	172.460	30	172.460	30
BB-3	1086.100	30	1086.100	30	1086.100	30
Survey	965.440	30	965.440	30	965.440	30

Figure 24. Viking Lander Camera FC-2B Calibration Constants

Contamination Cover Out of Optical Path

Diode	Value 1	Temp 1	Value 2	Temp 2	Value 3	Temp 3
BB-2	1067.047	11	1078.198	19	1115.847	46
Blue	136.690	11	138.650	19	145.250	46
Green	125.730	11	127.450	19	133.260	46
Red	292.309	11	297.720	19	315.990	46
Sun	10000.001	11	10000.000	19	10000.001	46
BB-4	1032.198	11	1046.377	19	1094.217	46
BB-1	1090.957	11	1102.448	19	1141.207	46
IR-3	172.680	11	168.450	19	154.180	46
IR-2	112.310	11	111.840	19	110.270	46
IR-1	191.450	11	194.040	19	202.760	46
BB-3	1045.757	11	1062.897	19	1120.727	46
Survey	1001.117	11	1010.017	19	1040.037	46

Contamination Cover Within Optical Path

Diode	Value 1	Temp 1	Value 2	Temp 2	Value 3	Temp 3
BB-2	1138.461	11	1150.359	19	1190.526	46
Blue	144.691	11	146.766	19	153.752	46
Green	133.344	11	135.168	19	141.330	46
Red	310.923	11	316.679	19	336.112	46
Sun	10000.001	11	10000.000	19	10000.001	46
BB-4	1101.260	11	1116.388	19	1167.429	46
BB-1	1163.992	11	1176.252	19	1217.607	46
IR-3	185.281	11	180.742	19	165.431	46
IR-2	120.583	11	120.078	19	118.392	46
IR-1	205.320	11	208.097	19	217.449	46
BB-3	1115.792	11	1134.080	19	1195.782	46
Survey	1068.517	11	1078.017	19	1110.057	46

Figure 25. Viking Lander Camera Spare Calibration Constants

Contamination Cover Out of Optical Path

Diode	Value 1	Temp 1	Value 2	Temp 2	Value 3	Temp 3
BB-2	959.909	11	967.949	19	995.078	46
Blue	110.660	11	112.370	19	118.130	46
Green	101.480	11	103.160	19	108.820	46
Red	279.660	11	284.169	19	299.369	46
Sun	10000.001	11	10000.000	19	10000.001	46
BB-4	887.408	11	894.358	19	917.819	46
BB-1	895.878	11	908.349	19	950.449	46
IR-3	170.690	11	166.860	19	153.940	46
IR-2	104.720	11	103.640	19	100.000	46
IR-1	161.169	11	162.280	19	163.550	46
BB-3	875.169	11	882.219	19	906.009	46
Survey	864.489	11	864.479	19	864.459	46

Contamination Cover Within Optical Path

Diode	Value 1	Temp 1	Value 2	Temp 2	Value 3	Temp 3
BB-2	1024.222	11	1032.800	19	1061.747	46
Blue	117.117	11	118.927	19	125.023	46
Green	107.602	11	109.384	19	115.385	46
Red	297.448	11	302.245	19	318.411	46
Sun	10000.001	11	10000.000	19	10000.001	46
BB-4	946.848	11	954.264	19	979.295	46
BB-1	956.002	11	969.310	19	1014.235	46
IR-3	183.154	11	179.044	19	165.181	46
IR-2	112.431	11	111.272	19	107.364	46
IR-1	173.658	11	174.054	19	175.416	46
BB-3	933.804	11	941.325	19	966.710	46
Survey	922.744	11	922.733	19	922.713	46

Figure 26. Viking Lander Camera FC-3A Calibration Constants

Contamination Cover Out of Optical Path

Diode	Value 1	Temp 1	Value 2	Temp 2	Value 3	Temp 3
BB-2	1023.657	11	1029.417	19	1048.837	46
Blue	120.080	11	122.150	19	129.140	46
Green	114.170	11	116.140	19	122.770	46
Red	293.100	11	298.490	19	316.700	46
Sun	10000.001	11	10000.000	19	10000.001	46
BB-4	991.958	11	1000.977	19	1031.427	46
BB-1	1029.397	11	1037.457	19	1064.667	46
IR-3	180 268	11	175.260	19	157.130	46
IR-2	113.060	11	111.070	19	104.340	46
IR-1	175.220	11	175.810	19	177.800	46
BB-3	1027.377	11	1033.267	19	1053.147	46
Survey	973.188	11	973.589	19	974.929	46

Contamination Cover Within Optical Path

Diode	Value 1	Temp 1	Value 2	Temp 2	Value 3	Temp 3
BB-2	1092.248	11	1098.395	19	1119.117	46
Blue	127.098	11	129.289	19	136.687	46
Green	121.060	11	123.149	19	130.179	46
Red	311.809	11	317.643	19	336.916	46
Sun	10000.001	11	10000.000	19	10000.001	46
BB-4	1058.487	11	1068.112	19	1100.604	46
BB-1	1098.355	11	1106.955	19	1135.987	46
IR-3	193.459	11	188.084	19	168.627	46
IR-2	121.390	11	119.254	19	112.028	46
IR-1	187.921	11	188.554	19	190.688	46
BB-3	1096.291	11	1102.576	19	1123.790	46
Survey	1038.684	11	1039.110	19	1040.541	46

Figure 27. Viking Lander Camera FC-2A Calibration Constants

Contamination Cover Out of Optical Path

Diode	Value 1	Temp 1	Value 2	Temp 2	Value 3	Temp 3
BB-2	1145.277	11	1152.750	19	1176.089	44
Blue	157.470	11	160.500	19	169.960	44
Green	127.140	11	129.220	19	135.710	44
Red	311.250	11	316.440	19	332.640	44
Sun	10000.001	11	10000.000	19	10000.001	44
BB-4	1163.607	11	1173.388	19	1203.967	44
BB-1	1130.797	11	1140.427	19	1170.537	44
IR-3	204.910	11	197.530	19	174.470	44
IR-2	113.740	11	111.600	19	104.930	44
IR-1	193.320	11	193.250	19	193.040	44
BB-3	1077.827	11	1081.688	19	1093.737	44
Survey	1043.698	11	1043.698	19	1043.698	44

Contamination Cover Within Optical Path

Diode	Value 1	Temp 1	Value 2	Temp 2	Value 3	Temp 3
BB-2	1222.067	11	1230.041	19	1254.945	44
Blue	166.688	11	169.896	19	179.909	44
Green	134.856	11	137.063	19	143.947	44
Red	331.073	11	336.593	19	353.825	44
Sun	10000.001	11	10000.000	19	10000.001	44
BB-4	1241.590	11	1252.025	19	1284.655	44
BB-1	1206.577	11	1216.852	19	1248.981	44
IR-3	219.843	11	211.925	19	187.184	44
IR-2	122.127	11	119.831	19	112.669	44
IR-1	207.358	11	207.283	19	207.058	44
BB-3	1150.139	11	1154.257	19	1167.116	44
Survey	1113.980	11	1113.981	19	1113.981	44

Figure 28. Viking Lander Camera FC-1B Calibration Constants

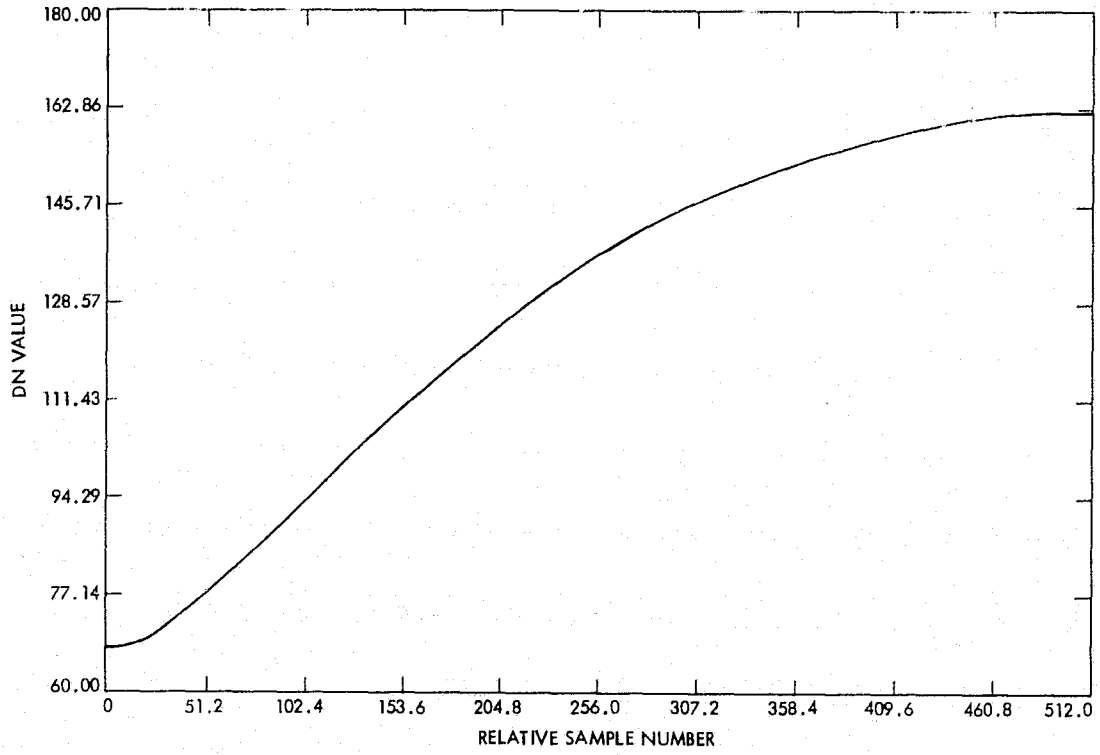

Figure 29. Calibration Lamp Ramp CAL 2

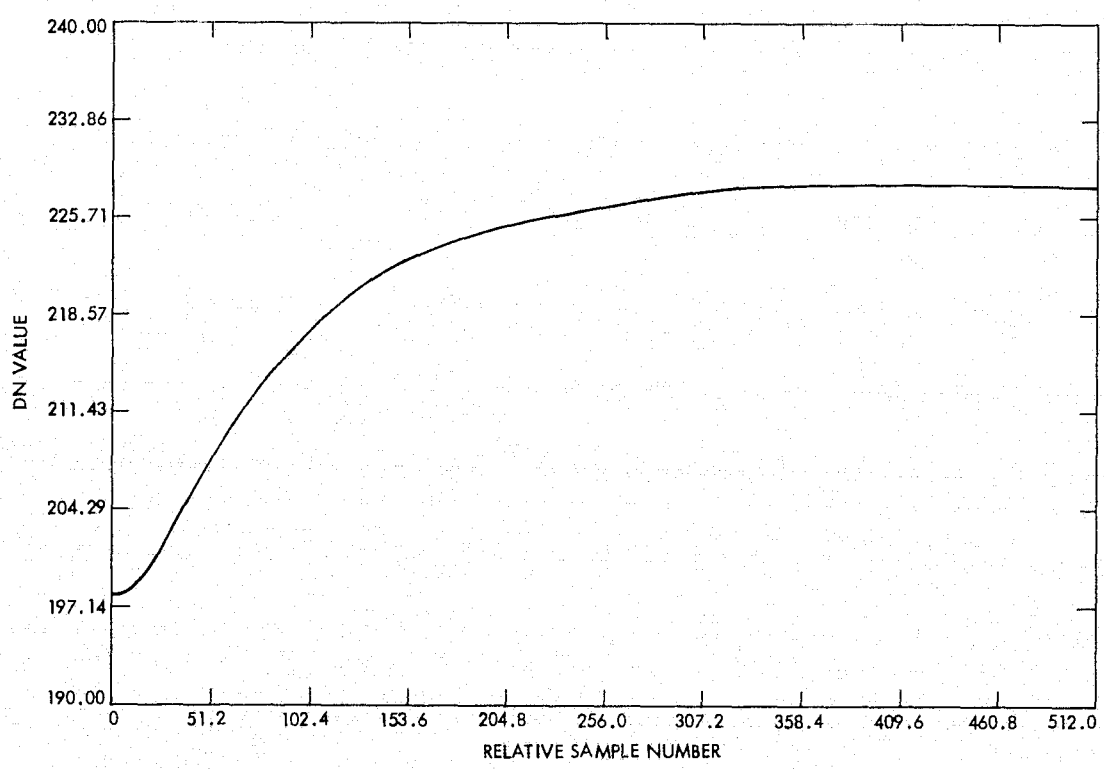

Figure 30. Calibration Lamp Ramp CAL 3

Calibration Number	Channel	Off	Gain	$\overline{DN}$	Sigma	File Number
2	BB1	1	1	30.420	1.416	31
3	BB1	1	2	28.900	0.965	32
2	BB2	1	1	28.050	1.126	33
3	BB2	1	2	29.740	0.611	34
2	BB3	1	1	37.450	1.099	35
3	BB3	1	2	36.600	0.568	36
2	BB4	1	1	36.860	1.096	37
3	BB4	1	2	39.650	0.623	38
2	Blue	1	0	35.460	7.735	39
3	Blue	1	1	29.530	3.925	40
2	Green	1	0	41.770	3.124	41
3	Green	1	1	40.220	1.426	42
2	Red	1	1	36.510	0.625	43
3	Red	1	2	40.060	0.370	44
2	IR1	1	1	34.120	1.203	45
3	IR1	1	2	33.200	0.617	46
2	IR2	1	1	25.950	1.417	47
3	IR2	1	2	21.270	0.646	48
2	IR3	1	1	25.050	1.081	49
3	IR3	1	2	18.370	0.560	50
2	Survey	1	1	36.880	0.517	51
3	Survey	1	2	38.450	0.498	52

Figure 31. FC-1B Internal Thermal Calibration Test

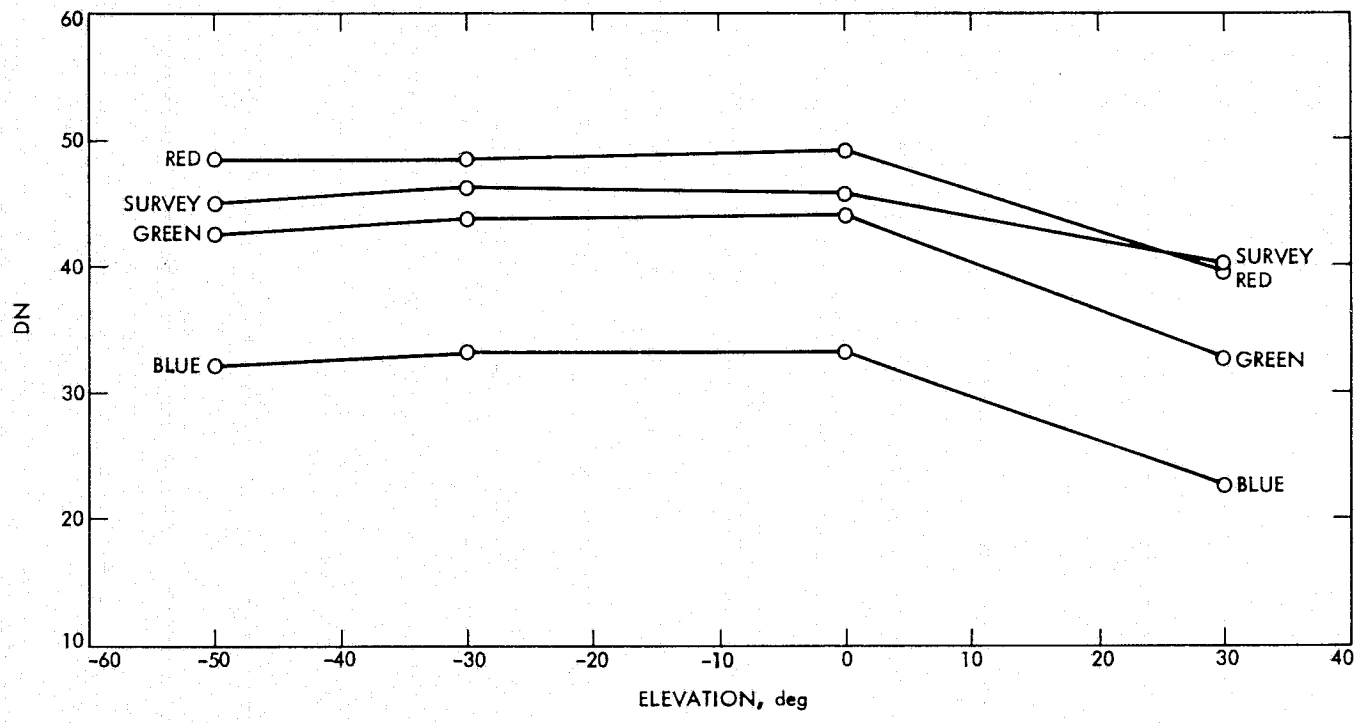

Figure 32. Spare Camera Color Response vs Elevation Angle, Contamination Cover Closed, Red, Green, Blue, Survey Diodes

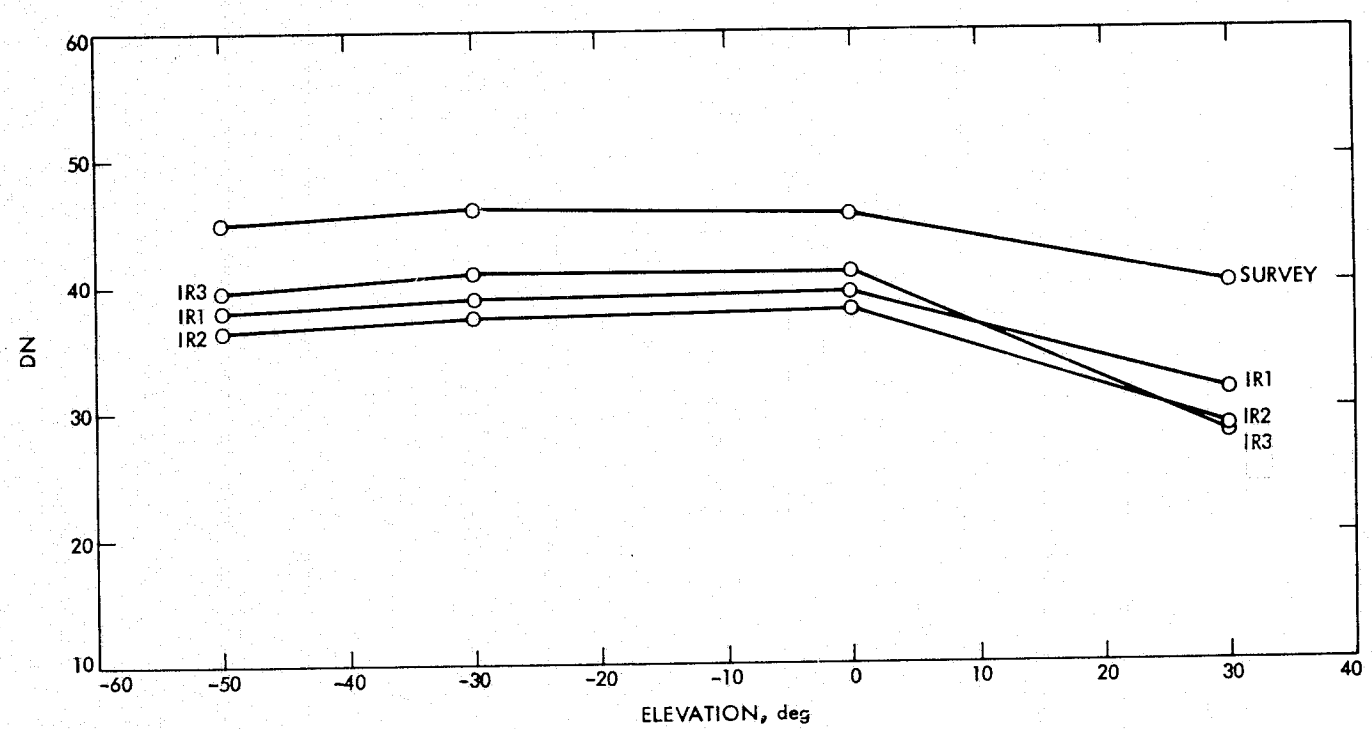

Figure 33. Spare Camera Color Response vs Elevation Angle, Contamination Cover Closed, IR1, IR2, IR3, Survey Diodes

Channel	Elevation, deg	Offset	Gain	Mean	Sigma
Red	0	1	4	49.167	1.069
Blue	0	1	4	33.167	0.688
Green	0	1	4	44.000	0.816
IR1	0	1	4	39.333	0.943
IR2	0	1	4	38.000	0.816
IR3	0	1	4	41.000	1.291
Survey	0	1	4	45.833	0.689
Red	+30	1	4	39.500	0.957
Blue	+30	1	4	22.500	0.500
Green	+30	1	4	32.333	0.746
IR1	+30	1	4	31.833	1.462
IR2	+30	1	4	28.333	1.106
IR3	+30	1	4	28.167	0.898
Survey	+30	1	4	40.000	0.816
Red	-30	1	4	48.500	3.452
Blue	-30	1	4	33.333	1.247
Green	-30	1	4	43.833	1.863
IR1	-30	1	4	39.000	1.826
IR2	-30	1	4	37.500	1.500
IR3	-30	1	4	41.000	0.816
Survey	-30	1	4	46.167	0.687
Red	-50	1	4	48.333	2.055
Blue	-50	1	4	32.167	0.688
Green	-50	1	4	42.667	1.248
IR1	-50	1	4	38.000	1.155
IR2	-50	1	4	36.667	1.247
IR3	-50	1	4	39.667	0.471
Survey	-50	1	4	45.000	0.577

Figure 34. Spare Camera Color vs Elevation Angle, Contamination Cover Closed

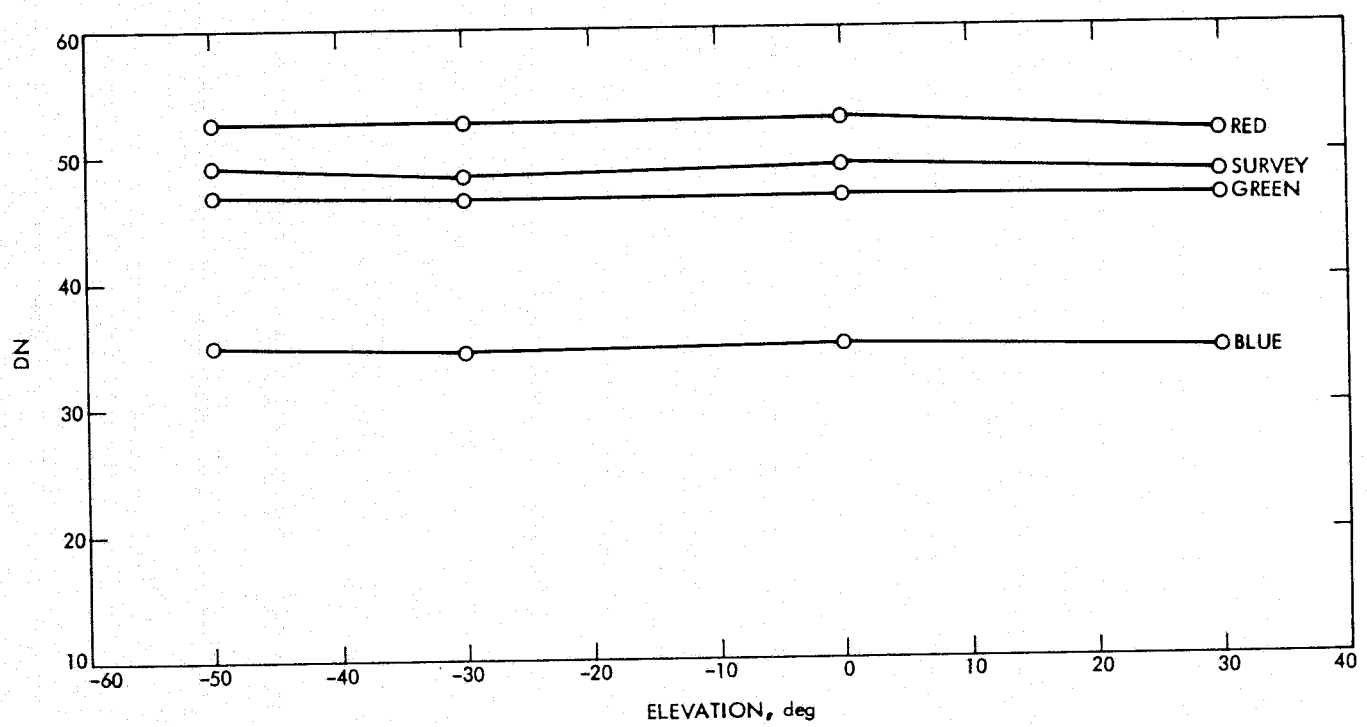

Figure 35. Spare Camera Color Response vs Elevation Angle, Contamination Cover Open, Red, Green, Blue, Survey Diodes

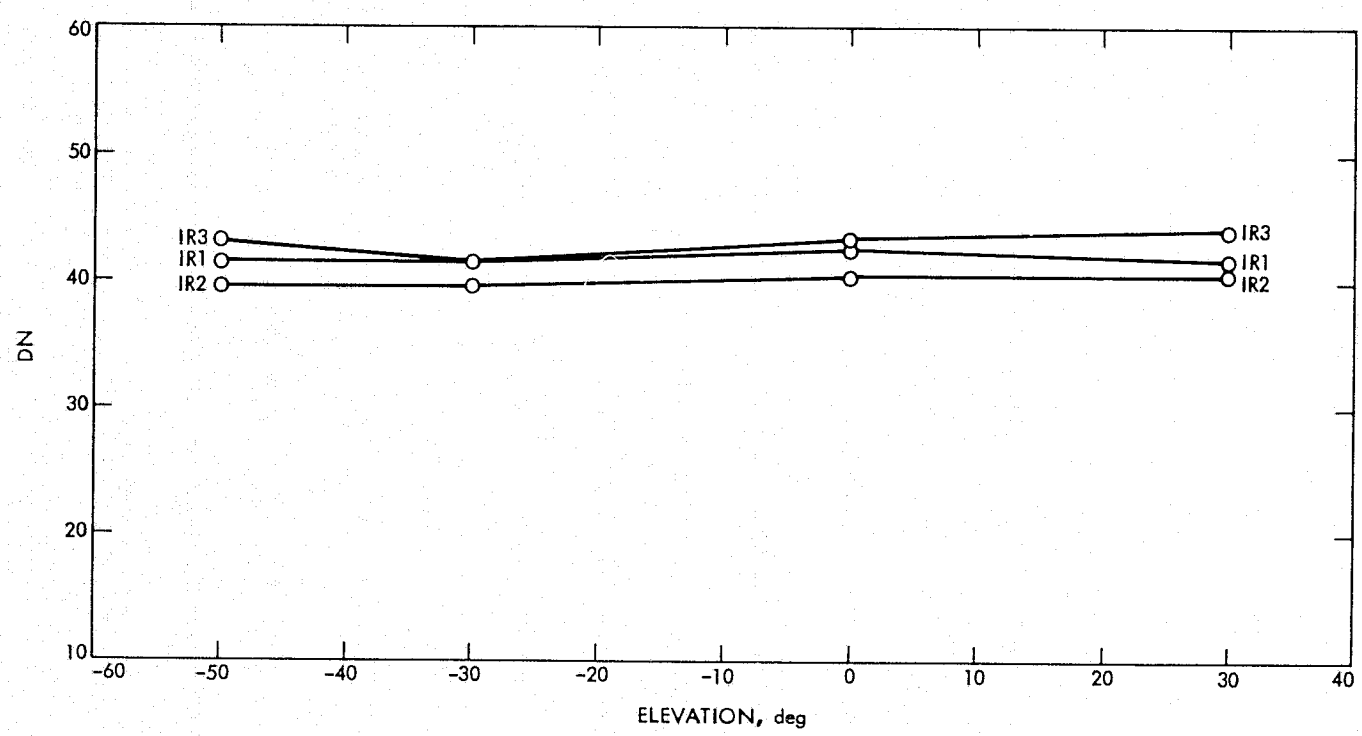

Figure 36. Spare Camera Color Response vs Elevation Angle, Contamination Cover Open, IR1, IR2, IR3 Diodes

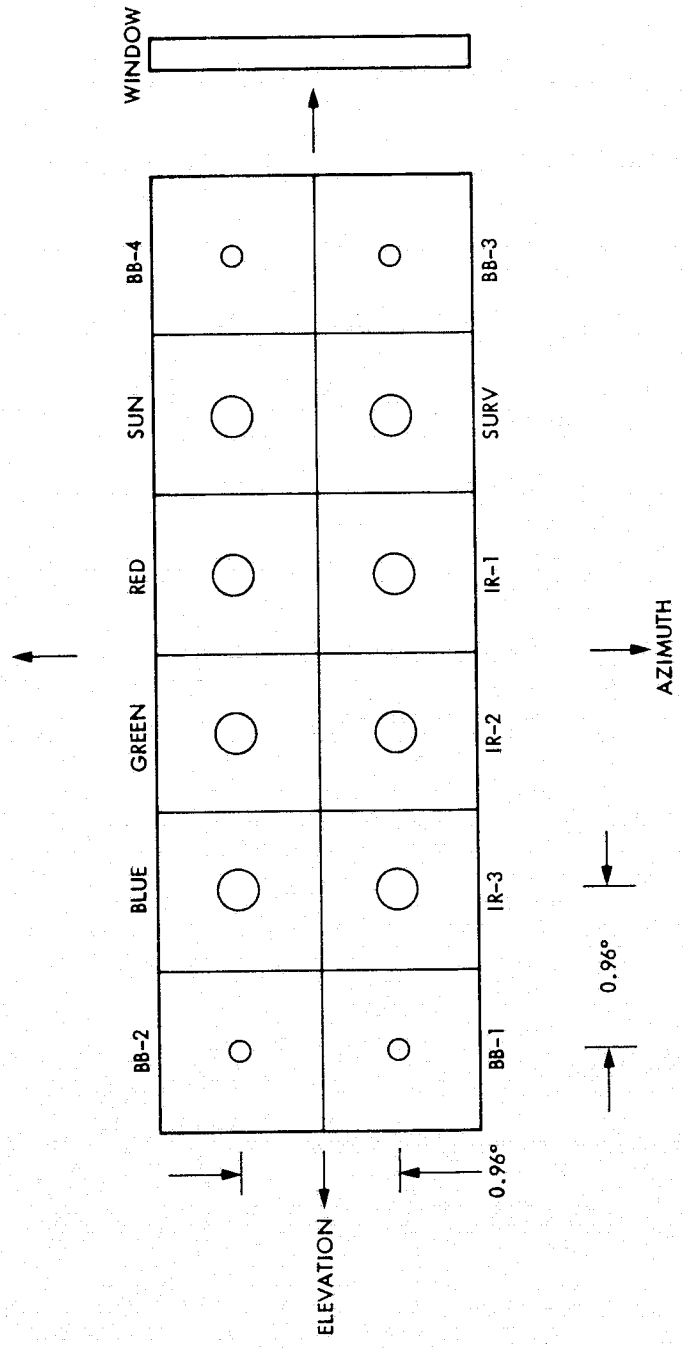

Figure 37. PSA Alignment Diagram

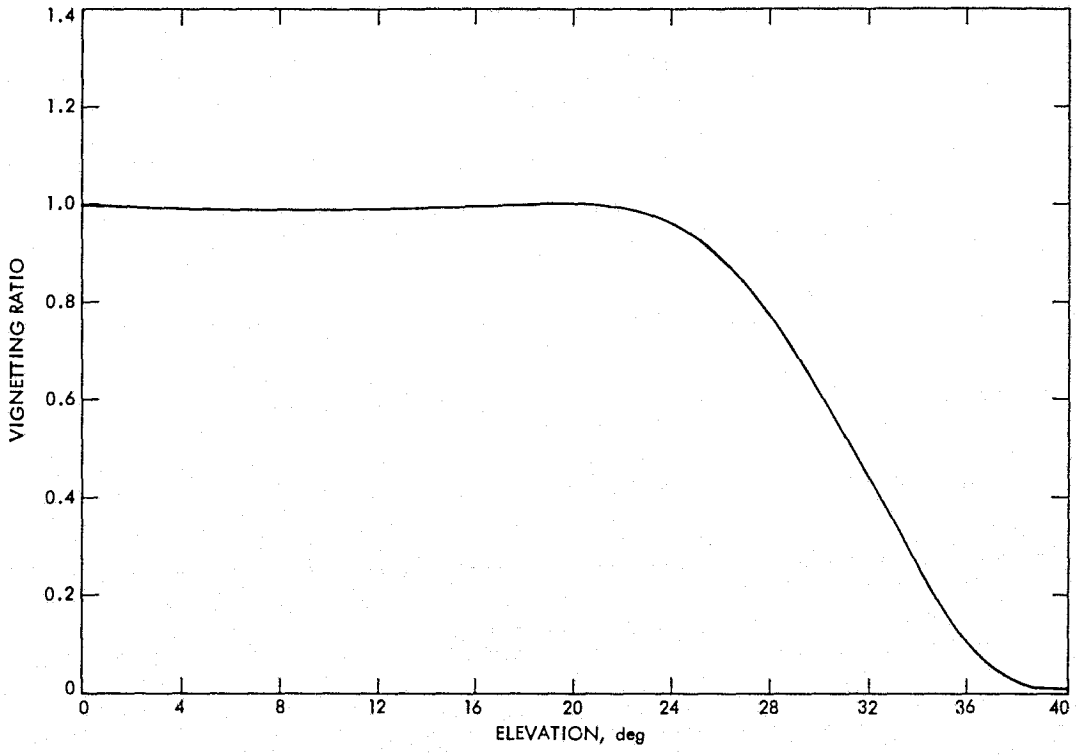

Figure 38. Vignetting Function, Blue Diode

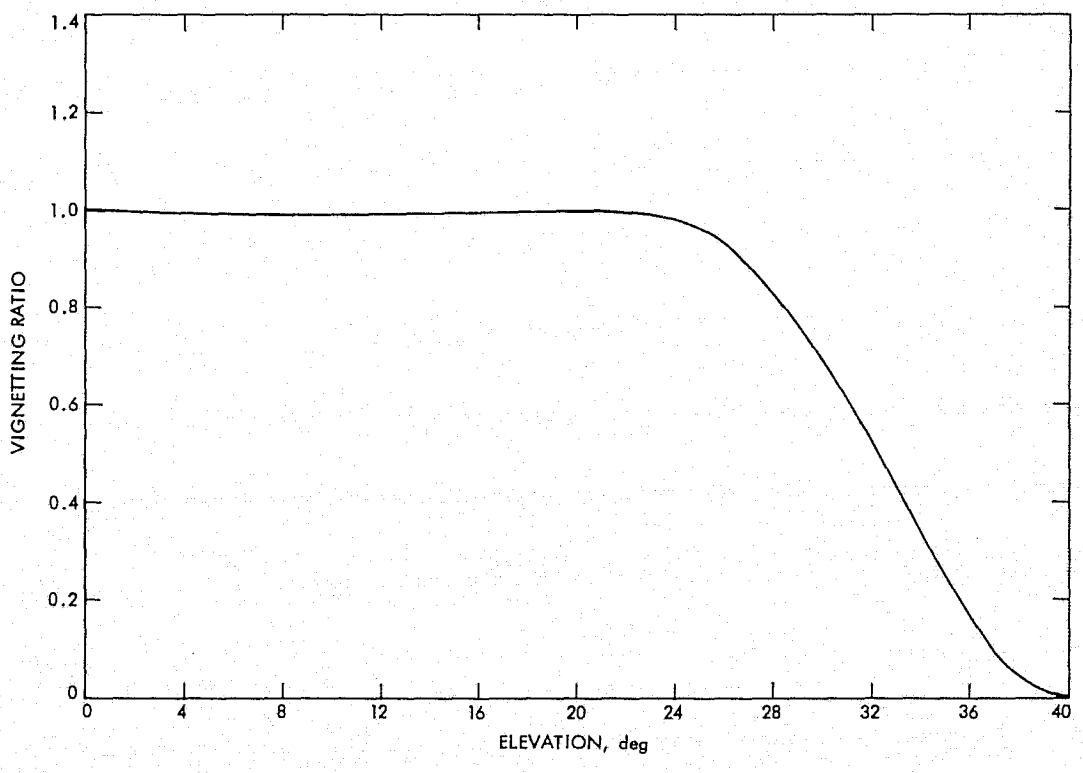

Figure 39. Vignetting Function, Green Diode

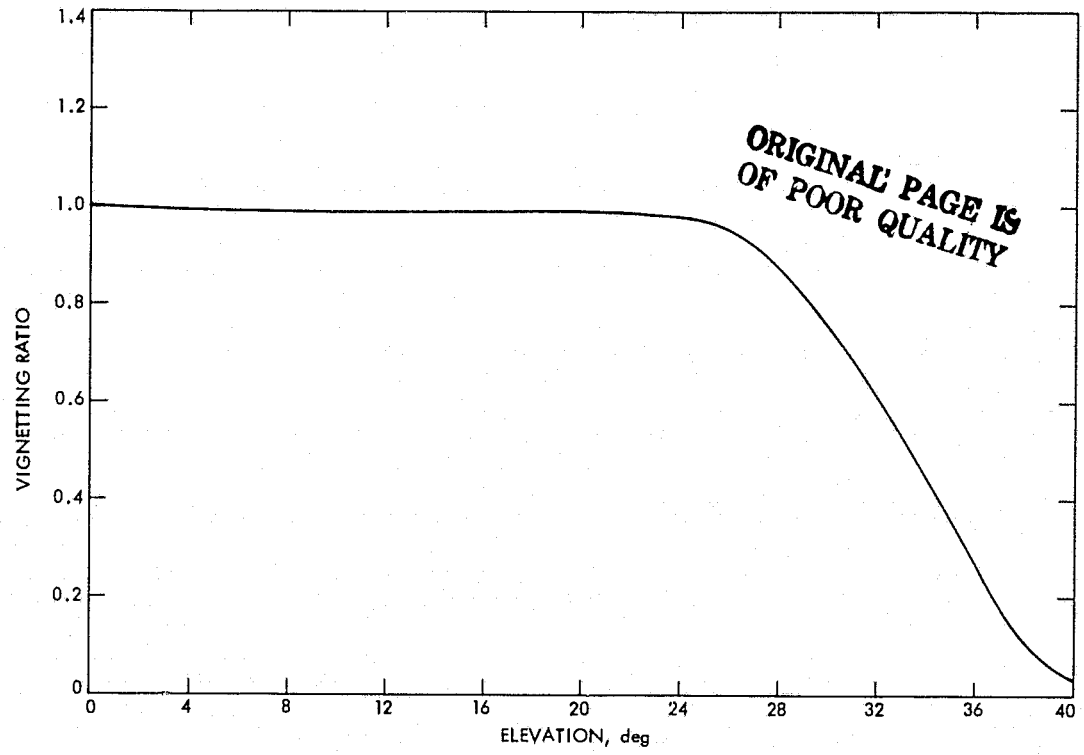

Figure 40. Vignetting Function, Red Diode

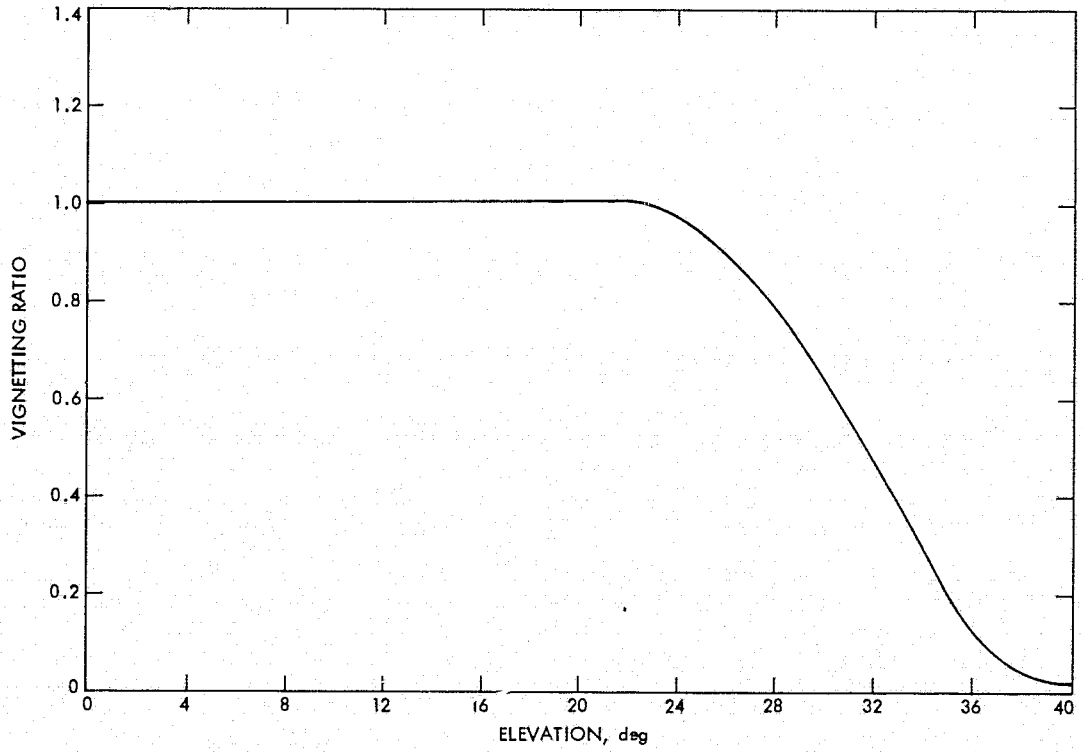

Figure 41. Vignetting Function, IR3 Diode

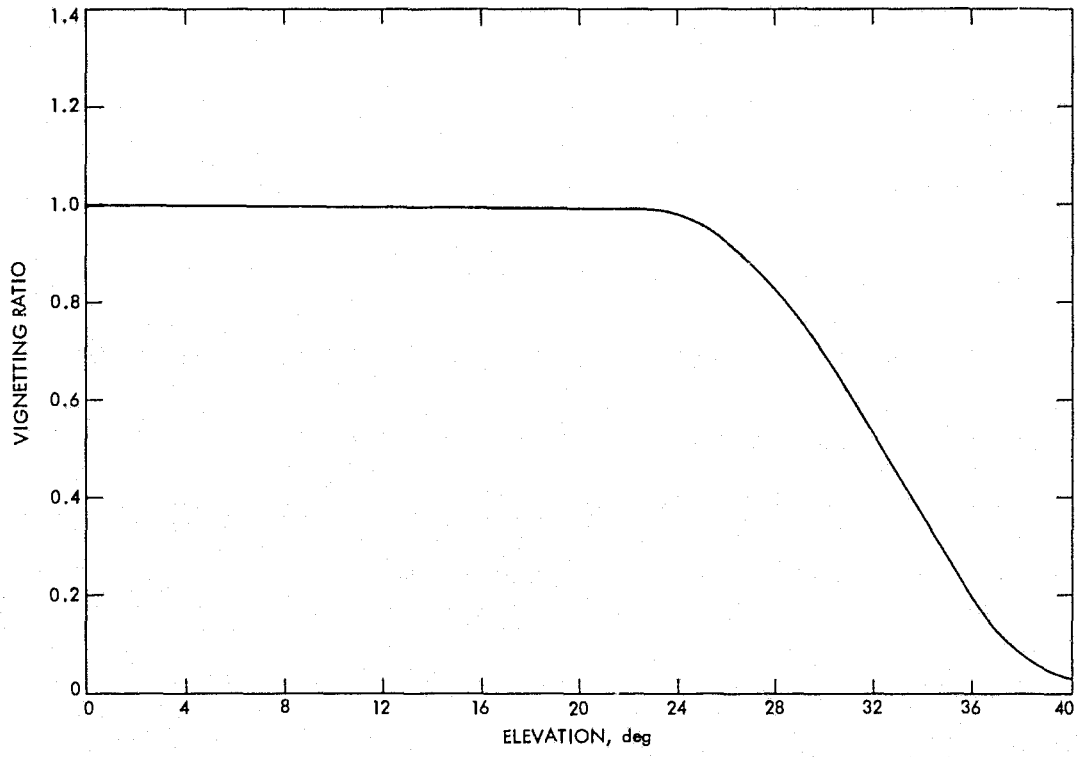

Figure 42. Vignetting Function, IR2 Diode

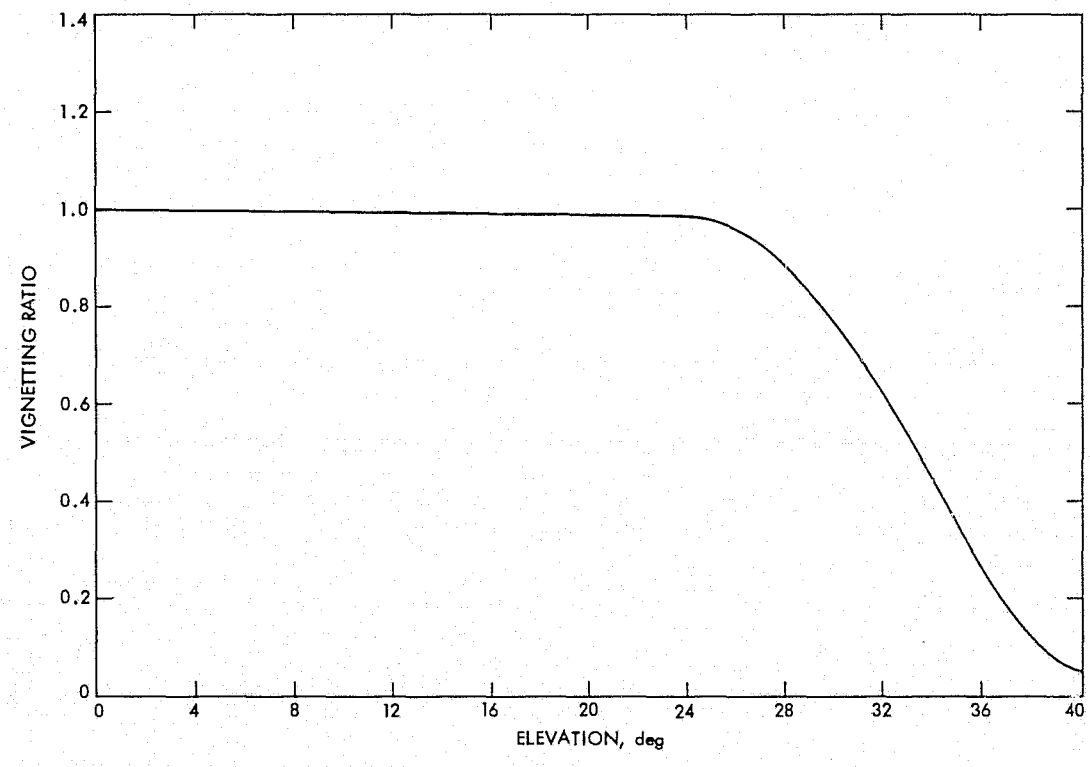

Figure 43. Vignetting Function, IR1 Diode

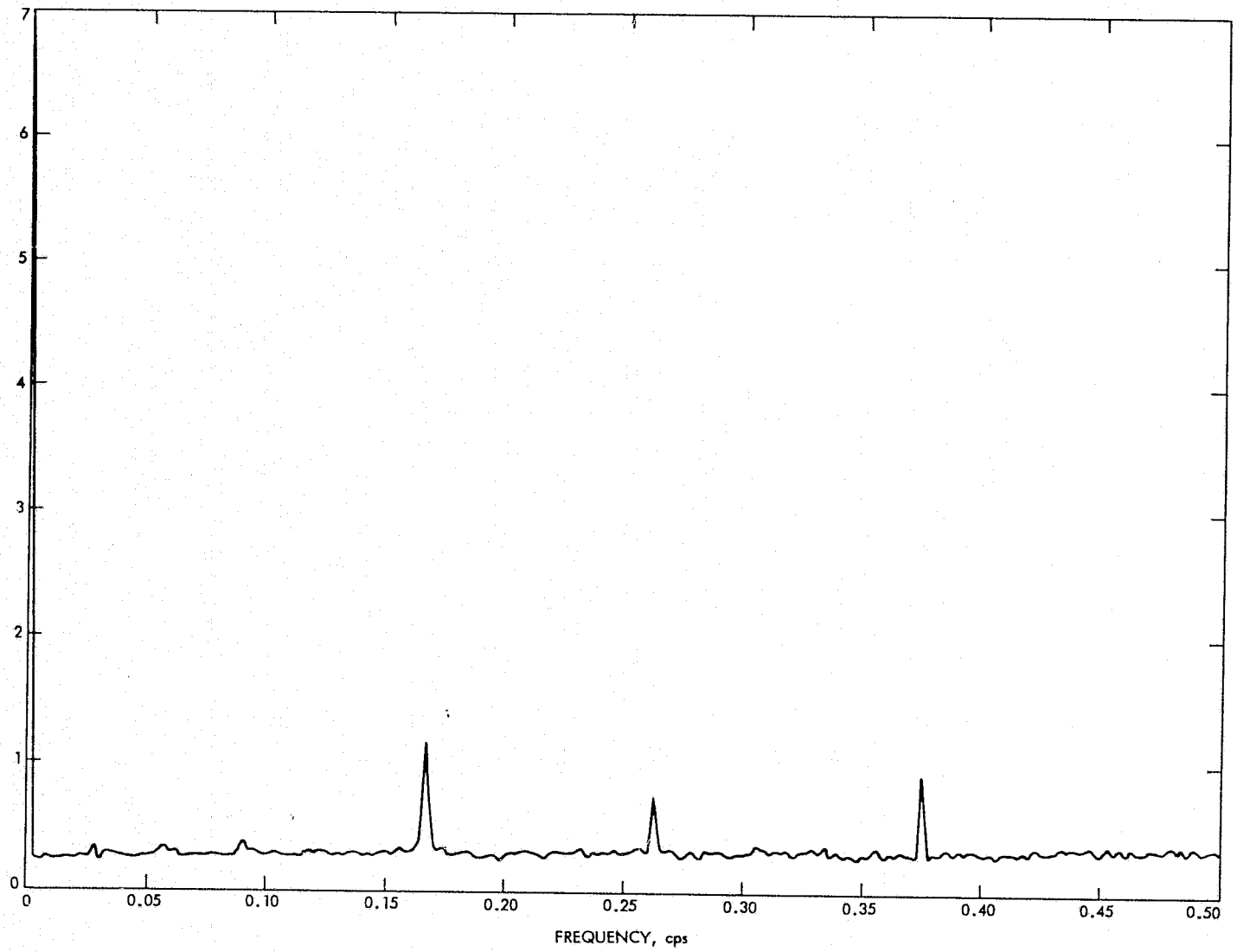

Figure 44. One-Dimensional Power Spectrum, Green Diode

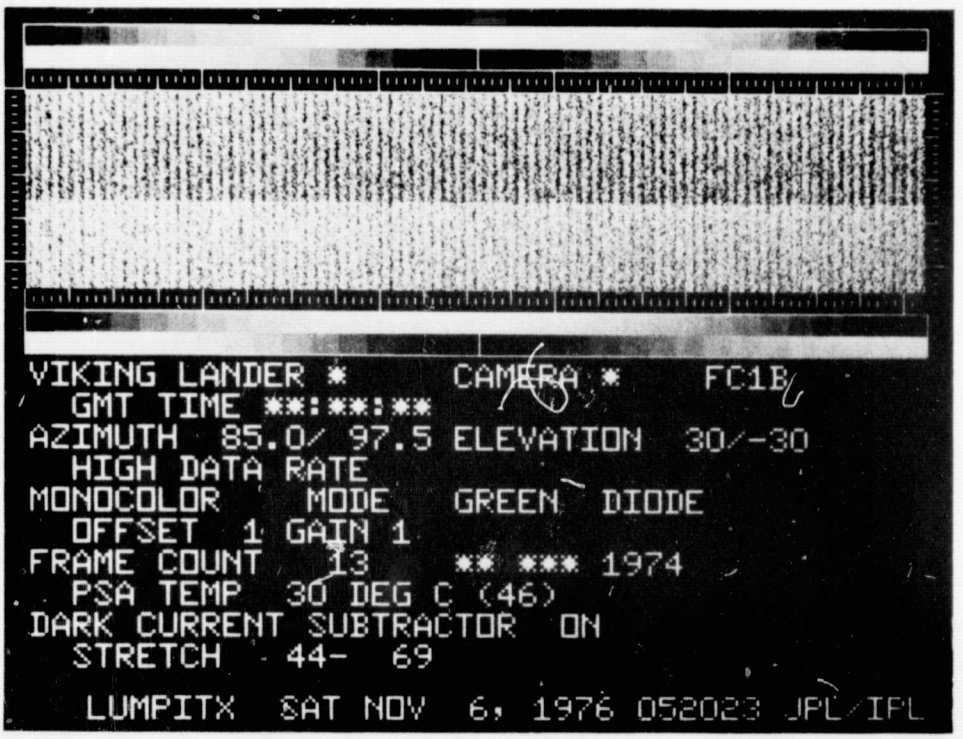

Figure 45. Coherent Noise Pattern, Green Diode

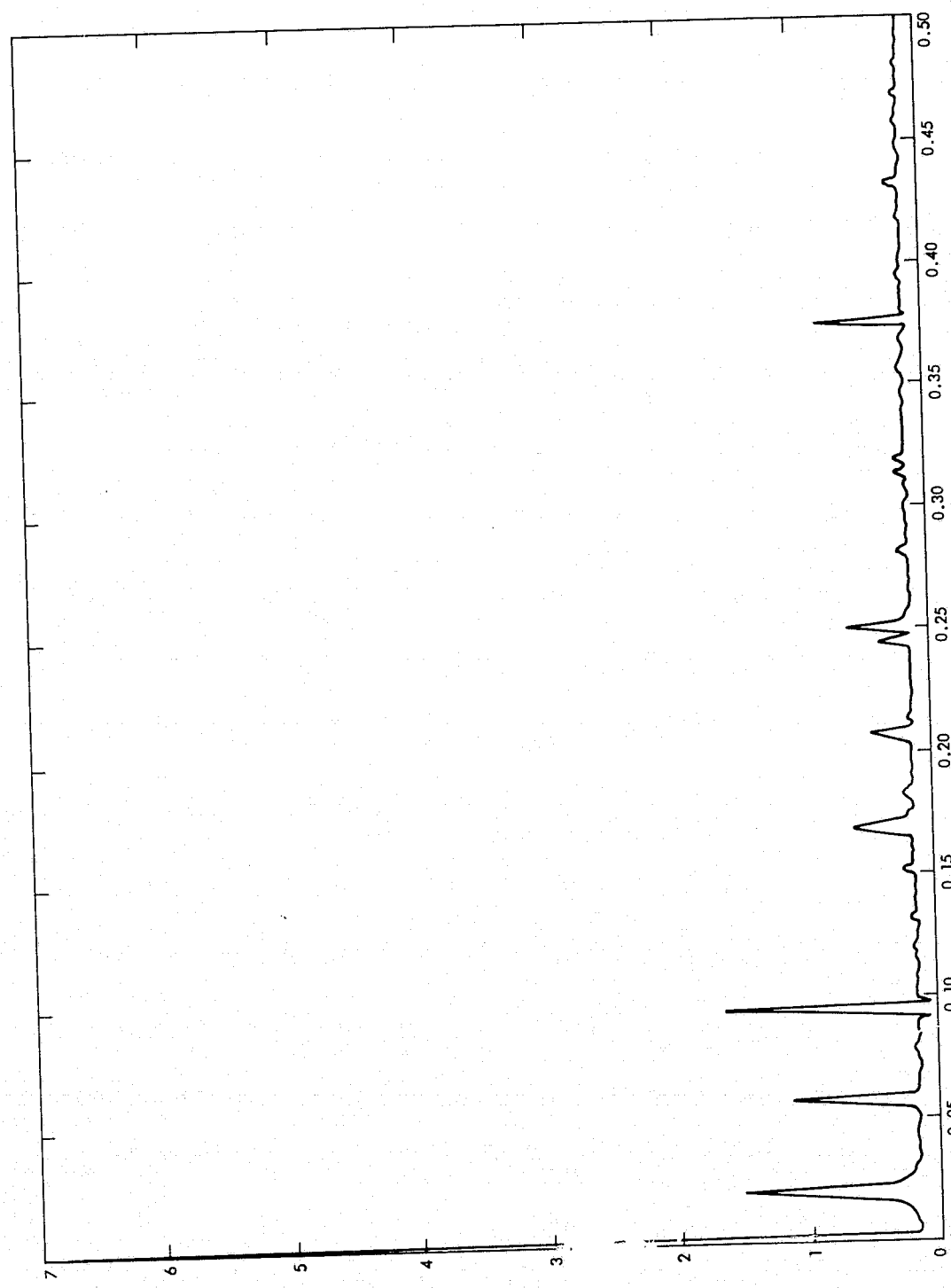

Figure 46. BB1 High Data Rate Power Spectrum

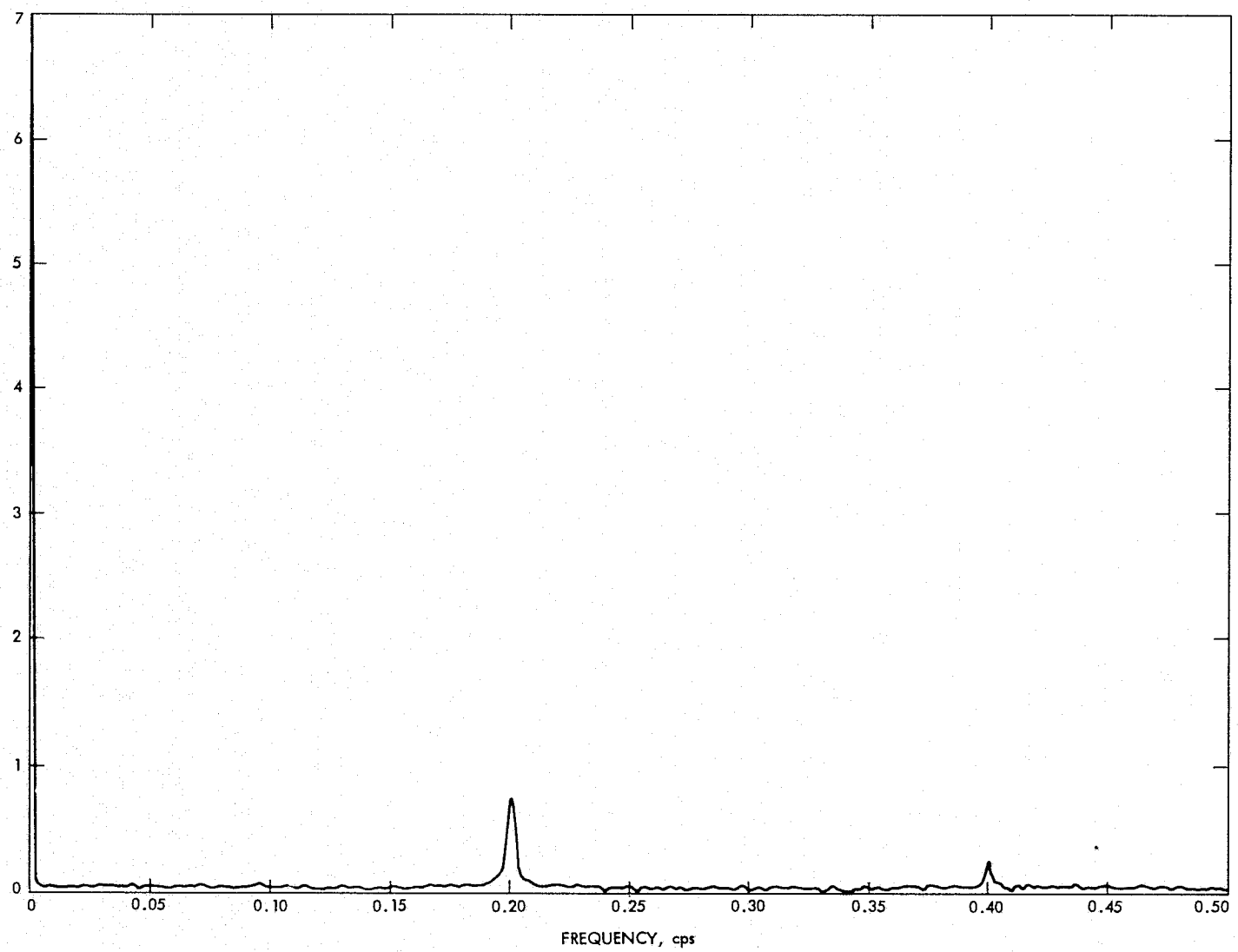

Figure 47. BB1 Low Data Rate Power Spectrum

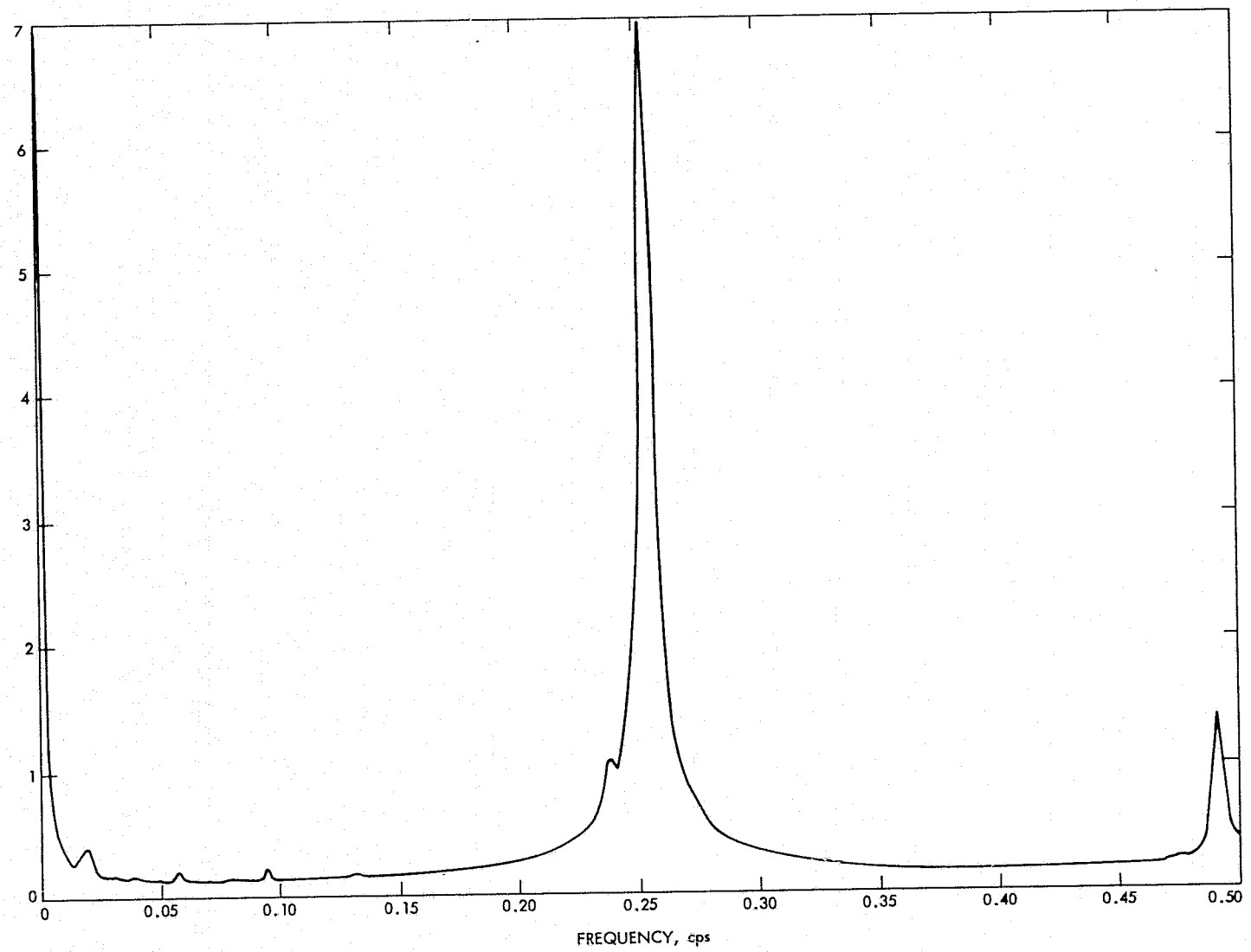

Figure 48. Power Spectrum Before Noise "Fix"

4	4	4	4	4	4	4	3	4	4	4	4	4	4	4	3	4	4
4	4	4	4	4	4	4	4	4	4	4	3	4	4	4	4	4	4
4	3	4	4	4	4	4	4	4	4	3	4	4	4	4	4	4	4
4	4	4	4	3	4	4	3	4	4	4	4	4	4	4	3	4	4
4	4	4	4	4	4	4	3	4	4	4	4	4	4	4	4	4	4
4	4	4	4	4	4	4	4	3	4	4	4	4	4	4	4	4	4
4	4	4	4	4	4	4	4	4	4	4	4	4	3	4	4	4	4
4	4	4	4	4	4	4	4	4	3	3	4	3	4	4	4	4	4
4	4	3	4	4	4	4	4	3	3	4	3	4	4	4	4	4	4
4	4	4	4	4	4	4	4	4	4	3	4	4	5	4	4	4	4
4	4	4	4	4	4	4	4	4	4	4	4	4	4	4	4	4	4
4	4	4	4	4	4	4	4	4	3	4	4	4	4	4	4	4	4
4	4	4	4	4	4	4	4	4	4	4	4	4	4	4	4	4	4
4	4	4	4	4	4	4	4	4	4	4	4	4	4	4	4	4	4
4	4	4	4	4	4	4	4	4	3	4	4	4	3	4	4	4	4
4	4	3	4	4	4	4	4	4	4	4	4	4	4	4	4	4	4
4	4	4	4	4	4	4	3	4	4	4	4	4	3	4	4	4	4
3	4	4	3	4	4	4	4	4	4	3	4	4	4	3	4	4	4
4	4	3	4	4	4	4	3	4	3	4	4	4	4	3	4	4	3
4	4	4	4	4	4	4	3	4	4	4	4	4	4	4	4	4	4
3	4	4	4	4	4	4	4	4	4	4	4	4	4	4	4	4	4
4	4	4	4	4	4	4	4	4	4	4	4	4	4	4	3	4	4
4	4	3	4	4	4	4	3	4	4	4	3	4	4	4	3	4	4
4	4	4	3	4	4	4	3	4	4	4	4	4	4	4	4	4	4
4	4	3	4	3	4	4	4	4	4	4	4	4	4	4	4	4	4
4	3	4	4	3	3	3	4	4	4	4	4	4	4	4	4	4	4
4	4	3	4	4	4	4	3	4	4	4	4	4	3	3	3	4	4
4	4	3	4	4	4	4	3	4	4	4	4	4	3	4	4	4	4
4	4	4	4	4	4	4	3	4	4	4	4	3	4	4	4	4	4
4	4	4	4	4	4	4	4	4	4	3	4	4	4	4	4	4	4
4	3	3	4	4	4	4	5	4	4	4	4	4	4	4	4	4	4
4	4	4	3	4	4	4	4	4	4	4	4	4	4	4	4	4	4
4	3	3	4	4	4	4	3	4	4	4	4	4	4	5	5	6	5
4	4	4	4	4	3	4	4	4	3	4	4	4	4	5	18	37	19
4	4	3	4	4	4	4	3	4	4	4	4	4	4	9	60	62	62
4	4	3	4	4	4	4	3	4	4	4	4	4	4	9	62	62	62
4	4	4	4	4	3	4	4	4	3	4	4	3	4	5	21	49	28
4	4	4	4	4	4	4	4	4	4	3	4	4	4	4	4	4	5
4	4	4	4	4	4	4	4	4	4	4	4	4	4	4	4	4	4
4	4	4	4	4	4	4	4	4	4	4	4	4	4	4	3	4	4
3	4	4	4	3	4	4	3	4	3	4	4	4	4	4	3	4	4
4	3	4	4	4	4	4	4	4	4	4	4	4	4	4	4	4	4
4	4	3	4	4	4	4	3	4	4	4	4	4	4	4	4	4	4
4	4	4	3	4	4	4	3	4	4	4	4	4	4	4	4	3	4
4	4	4	4	3	4	4	4	4	3	4	4	4	4	4	4	4	4
4	4	4	4	3	3	4	4	4	4	4	4	4	4	4	4	4	4
4	4	4	4	4	4	4	4	4	4	4	4	4	4	4	4	4	4
4	4	4	4	4	3	4	4	4	3	4	4	4	4	4	3	4	4
4	4	4	4	4	4	4	4	4	4	4	4	4	4	4	4	4	4
4	4	4	4	4	3	4	4	4	4	4	4	4	4	4	4	4	4

Figure 49. Point Spread Function — BB3 Primary Peak

50	4	4	4	4	4	4	4	4	3	4	4	4	4	4	4	4	4
51	3	3	4	4	4	4	4	4	3	4	4	4	4	4	4	4	4
52	4	4	4	4	4	4	4	4	4	4	4	4	4	3	4	4	4
53	4	4	4	4	5	4	4	4	4	4	4	4	4	4	4	4	4
54	4	4	4	4	4	4	4	4	4	4	4	4	4	4	4	4	4
55	3	4	4	4	4	4	4	4	3	4	4	4	4	4	4	4	4
56	4	3	4	4	4	4	3	4	4	4	4	4	4	4	4	4	4
57	4	4	4	4	4	4	4	4	3	4	4	4	4	4	4	4	4
58	4	4	4	4	4	4	4	4	3	4	4	4	4	4	3	4	4
59	4	3	4	4	3	4	4	4	4	4	4	4	4	4	4	4	4
60	4	4	4	3	4	4	4	4	4	4	3	4	4	4	4	4	4
61	4	4	4	4	4	4	3	4	4	4	4	4	4	4	4	4	4
62	4	3	4	4	4	4	4	4	3	4	4	3	4	4	4	4	4
63	4	4	4	4	4	4	4	4	4	4	4	4	4	4	4	4	4
64	4	4	4	4	4	4	4	4	4	4	4	4	4	4	4	4	4
65	4	4	4	3	4	4	3	4	4	4	4	4	4	4	3	4	4
66	4	4	4	3	4	4	3	4	3	4	4	4	4	4	4	4	4
67	3	4	4	4	4	4	4	4	3	4	4	4	3	4	4	3	4
68	4	3	4	4	4	4	4	4	4	3	4	4	4	4	3	4	4
69	3	4	4	3	4	4	3	4	4	4	4	4	4	4	4	4	4
70	3	4	4	3	4	4	4	4	4	3	4	4	3	4	4	4	4
71	3	4	4	4	4	4	4	4	3	4	4	4	4	4	4	4	4
72	4	4	4	4	4	4	3	4	4	4	4	4	4	4	3	4	4
73	4	4	4	3	4	4	4	5	3	4	4	3	4	4	4	3	4
74	4	4	4	4	4	3	4	4	4	4	4	4	4	4	3	4	3
75	4	4	4	4	4	4	4	4	4	4	4	4	4	3	4	4	3
76	4	4	4	5	4	4	4	4	4	3	4	4	4	4	3	4	4
77	4	4	3	3	4	4	4	4	4	4	4	4	4	4	3	4	4
78	4	4	4	4	4	4	4	4	3	4	4	4	4	4	4	4	4
79	4	4	3	4	4	4	4	3	4	4	4	4	4	4	4	4	4
80	4	4	3	4	4	4	4	4	3	4	4	4	4	3	3	4	4
81	4	4	4	4	4	3	4	4	4	4	4	4	4	4	4	3	4
82	4	4	4	4	4	4	4	4	3	4	4	4	4	3	3	4	4
83	4	4	4	5	4	4	4	4	4	3	4	4	4	4	4	4	4
84	4	5	5	5	4	4	4	4	3	3	4	4	4	4	3	4	4
85	4	5	5	4	4	3	4	4	3	4	4	3	4	4	3	4	4
86	4	4	4	4	4	3	4	4	3	4	4	4	4	4	4	4	4
87	4	4	4	4	3	4	4	4	4	4	4	4	4	4	4	4	4
88	4	4	3	4	4	4	4	4	3	4	4	4	4	4	4	4	4
89	3	4	4	3	4	4	4	3	3	4	4	4	4	4	4	4	4
90	3	4	4	4	4	4	4	4	4	4	4	4	3	4	4	4	3
91	4	3	4	4	4	4	3	4	4	3	4	4	4	3	4	4	4
92	4	4	4	4	4	4	3	4	4	4	4	3	4	4	3	4	4
93	4	4	4	4	4	4	4	4	4	4	4	4	4	4	4	3	4
94	4	4	4	4	3	4	4	4	4	4	4	4	4	4	4	4	3
95	4	4	4	4	4	4	4	4	4	4	4	4	4	4	4	4	3
96	4	4	4	3	4	4	4	4	3	4	4	3	4	4	4	4	4
97	4	4	4	3	4	3	4	3	4	4	4	4	4	4	4	4	4
98	4	5	4	4	4	5	4	4	4	4	4	4	4	4	4	4	4
99	4	3	4	4	4	4	5	4	4	4	4	4	4	4	4	4	4

Figure 50. Point Spread Function — BB3 Secondary Peak

50	7	8	6	5	6	7	8	7	7	7	7	7	8	8	7
51	6	6	5	6	6	7	7	8	7	8	9	8	7	6	6
52	7	7	7	6	7	6	6	7	5	6	7	7	6	6	6
53	8	7	5	5	6	7	6	7	7	7	6	7	7	7	6
54	6	8	8	7	8	7	8	9	8	7	8	7	6	6	5
55	7	7	8	5	6	6	6	7	7	7	7	6	6	8	7
56	7	8	6	5	6	6	6	8	7	6	8	8	8	7	6
57	7	8	7	7	7	6	6	7	6	6	6	6	8	6	5
58	8	7	8	5	6	6	7	5	6	9	7	6	8	8	8
59	7	6	7	7	8	7	7	8	7	8	9	7	8	6	6
60	8	8	7	6	6	6	7	7	7	6	7	7	8	7	8
61	7	7	6	6	7	6	7	7	8	9	7	8	8	9	6
62	7	8	7	7	8	7	7	8	7	7	6	6	8	7	6
63	8	8	8	6	7	8	11	13	11	8	8	8	7	7	6
64	8	7	8	7	10	19	47	58	36	14	10	8	9	7	6
65	8	7	9	8	10	39	62	62	62	32	9	7	7	8	6
66	5	6	7	7	15	62	62	62	62	25	8	7	8	8	7
67	7	7	8	8	8	31	62	62	62	16	7	6	7	7	6
68	7	7	9	7	7	8	21	30	18	6	6	7	7	7	5
69	6	6	7	7	7	7	8	9	7	7	8	7	8	7	7
70	7	7	8	7	8	7	6	6	5	7	6	6	7	7	6
71	4	6	6	6	7	6	7	7	5	5	7	7	7	7	7
72	6	7	7	7	7	7	6	7	7	6	6	6	6	5	6
73	6	7	8	6	6	5	6	6	5	5	4	5	7	7	6
74	6	6	7	7	6	8	6	7	6	7	7	7	8	8	8
75	7	7	7	7	7	8	7	7	5	6	7	6	7	6	7
76	6	5	6	7	7	6	7	5	5	5	6	7	7	7	6
77	4	7	6	6	6	7	7	7	8	5	7	6	6	7	5
78	7	7	7	7	8	6	7	6	5	5	5	4	6	8	7
79	5	7	7	6	7	6	7	7	8	6	7	7	7	7	7
80	6	6	7	7	9	7	8	7	7	6	5	5	7	6	6
81	6	6	7	5	6	7	5	6	5	5	7	6	7	7	6
82	5	6	6	6	6	7	7	6	5	6	6	5	6	7	6
83	7	6	6	7	8	7	7	7	6	5	5	5	5	5	7
84	5	7	6	5	7	6	7	7	8	7	8	6	7	7	7
85	6	6	6	6	7	8	8	8	6	6	6	5	7	6	6
86	5	6	7	5	8	7	8	8	6	6	6	6	6	7	6
87	5	5	5	6	6	8	10	10	7	6	7	5	7	6	5
88	8	7	5	7	8	9	10	10	6	6	5	5	5	5	5
89	6	6	8	6	7	7	7	7	7	6	7	7	6	7	6
90	6	5	6	6	6	7	9	8	7	8	7	6	6	6	7
91	6	5	6	6	6	6	7	7	6	6	5	5	5	7	7
92	5	6	5	5	5	6	7	7	7	6	7	6	7	6	5
93	7	7	5	6	7	7	7	7	6	8	5	5	7	6	5
94	6	5	7	5	5	6	7	7	7	7	7	6	6	7	6
95	6	6	6	6	6	6	7	10	6	7	8	6	6	6	5
96	7	7	5	6	7	6	6	5	6	7	7	5	6	5	6
97	5	6	5	5	6	5	7	7	7	7	8	6	6	6	6
98	6	6	7	7	6	7	7	8	7	7	7	6	6	6	6
99	8	7	6	6	8	6	6	7	7	7	6	8	7	7	7

Figure 51. Point Spread Function — Green